UNIVERSITY OF CALIFORNIA SAN DIEGO

# Chemistry of Indoor-Relevant Carboxylic Acids on Titanium Dioxide Surfaces

A Thesis submitted in partial satisfaction of the requirements
for the degree Master of Science

in

Chemistry

by

Renee Lillian Tam

Committee in charge:

Professor Vicki H. Grassian
Professor Jeffrey Rinehart
Professor Wei Xiong

2019

The Thesis of Renee Lillian Tam is approved, and it is acceptable in quality and form for publication on microfilm and electronically:

_____

_____

_____

Chair

University of California San Diego

2019

# DEDICATION

To my parents and grandparents – my constant beacons of inspiration,

One destination has been reached, but in the words of Nipsey Hussle, “the marathon continues”.

TABLE OF CONTENTS

LIST OF FIGURES

LIST OF TABLES

# ACKNOWLEDGEMENTS

First and foremost, I want to thank my advisor, Professor Vicki Grassian, for providing me the opportunity to do graduate-level research in her group. I came into her group with limited chemistry research experience, but Professor Grassian still took a chance and allowed me to pursue a research-focused Master's degree. I definitely would not have been able to graduate with this degree if it was not for her continuous patience and support. Even with her busy schedule, Professor Grassian always made time to meet with me to discuss data and provide guidance for any uncertainties I had. It has been a blessing to work with an advisor who is as supportive and knowledgeable as Professor Grassian, and I will be forever grateful for the opportunities she has given me.

My graduate-research experience would not have been the same without the support from the past and current members of the Grassian group. First, I want to thank my two mentors: Dr. Mona Shrestha and Dr. Yuan Fang. Dr. Shrestha taught me how to become an independent researcher, pushed me to think critically, and was supportive and patient with me when I felt confused and overwhelmed. Dr. Fang trained me on how to use the ATR-FTIR and was always available to answer any of my questions even though she was busy with her own research projects. Secondly, I want to thank Dr. Natalia Gonzalez-Pech for training me on how to use the QCM-D and Haibin Wu for allowing me to use his computer to analyze my QCM-D data. Next, I want to thank Man Luo, Victor Or, and Izaac Sit for being a part of my "6pm club" during the last six months of my Master's program. They are the ones who kept me company during the long work days, allowed me to think out loud, answered my questions, and made my last moments of graduate school a little less stressful. To the rest of the Grassian group members, thank you for being wonderful friends and a joy to work with.

Last, but not least, I want to thank my family and friends for their endless support. Thank you to my mom and dad for encouraging me to pursue a higher education, teaching me the importance of good work ethic, and keeping me in their prayers during the good and bad times. Thank you to my boyfriend, Dale Lee, and my two closest friends, Jessica Ma and Kari Tatoian, for keeping me sane by being my escape during the weekends and picking up the phone to talk whenever I need to just de-stress. And of course, thank you God for continuously watching over me and blessing me – all of this was done through Him.

Chapter 3, in full, is currently being prepared for submission for publication of the material. Tam, R. L.; Shrestha, M.; Grassian, V. H. Surface Chemistry and Adsorption Kinetics for Indoor Relevant Carboxylic Acids in Aqueous Solutions onto $TiO_2$ Nanoparticles: A Study of pH. The thesis author is the primary investigator and author of this paper.

Chapter 4, in full, is currently being prepared for submission for publication of the material. Tam, R. L.; Shrestha, M.; Grassian, V. H. Surface Chemistry and Adsorption Kinetics for Indoor Relevant Carboxylic Acids in Aqueous Solutions onto $TiO_2$ Nanoparticles: A Study of pH. The thesis author is the primary investigator and author of this paper.

ABSTRACT OF THE THESIS

Chemistry of Indoor-Relevant Carboxylic Acids on Titanium Dioxide Surfaces

by

Renee Lillian Tam

Master of Science in Chemistry

University of California San Diego, 2019

Professor Vicki H. Grassian, Chair

Compounds identified in indoor air are emitted from various sources like cooking, cleaning products, and human metabolism. Since a majority of homes experience dampness, these gaseous compounds can partition into the aqueous phase. Chemical interactions between these compounds and surfaces play an important role in altering the composition of indoor air, yet there is still a lack of knowledge on the mechanisms behind indoor surface chemistry. $TiO_2$ is a major component of paints and self-cleaning surfaces and, therefore, of interest in indoor air

chemistry. The adsorption of two indoor-relevant carboxylic acids, lactic acid and pyruvic acid, onto $TiO_2$ particle surfaces is investigated in the aqueous phase at acidic and indoor-relevant pH values. Specifically, by using attenuated total reflection-FTIR spectroscopy coupled with quartz crystal microbalance with dissipation, this thesis focuses on the surface chemistry of lactic and pyruvic acid on $TiO_2$, including adsorption kinetics, surface coverage, and speciation as a function of pH. The results conclude that lactic and pyruvic acid deprotonate upon adsorption and bind to $TiO_2$ via bidentate bridging. Adsorption and desorption rate constants do not differ significantly when pH changes. Surface coverage is dependent on solution pH and decreases with increasing pH. Solution and surface speciation for lactic acid remain constant as a function of pH, but solution and surface speciation differ for pyruvic acid at higher pH values, suggesting that surface adsorption induces a change in species equilibrium. An overall molecular picture emerges from these studies of the adsorption of these important organic acids on $TiO_2$ surfaces.

# Chapter 1 Introduction to Indoor Air Environments

The modern human spends, on average, 80 – 90% of the day within indoor environments, and a majority of that time is spent in one's own residence.[1] Therefore, the pollutants found in indoor air and the chemistry within indoor environments can immensely impact personal exposure;[2] yet, the amount of research regarding indoor air is still limited in comparison to outdoor air research. During the past two decades, roughly 300 papers on chemistry in indoor environments were published, while the number of publications on chemistry in outdoor environments surpassed 12,000.[9] Although discoveries concerning atmospheric processes can contribute to our understanding of indoor chemistry, indoor environments have different conditions than outdoor environments that can affect its chemistry. Firstly, indoor environments contain many variable characteristics, such as temperature variability, light, relative humidity, and ventilation.[9] Secondly, chemical transformations in indoor environments can occur in a variety of ways: in the gas-phase, on particles, and on indoor surfaces. Lastly, indoor environments can release different types and a higher magnitude of emissions than the outdoors. For example, cyclomethylsiloxanes ($C_{10}H_{30}O_5Si_5$ and $C_{12}H_{36}O_6Si_6$) are common indoor compounds that are emitted from personal care products. Formaldehyde (HCHO), which is produced in the atmosphere through photochemical reactions with hydrocarbon pollutants and directly emitted indoors from plywood, glues in furniture, and carpet shampoos, has lower emissions outdoors than indoors, with concentrations of 12.53 ppb and 54.56 ppb, respectively.[11,12] Thus, indoor chemistry, a complex phenomenon due to the diversity of emission sources and chemical transformation conditions, is necessary to understand in order to

comprehend indoor air composition, assess occupants' exposure, and identify potential adverse health effects.

## 1.1 Sources of Indoor Air Pollutants

The pollutants in indoor environments are a mixture of compounds introduced from the outdoors and emitted from indoor sources.[1] While ventilation can transport biogenic and anthropogenic-generated volatile organic compounds from outdoors to indoors,[3] previous studies demonstrate that the level of volatile organic compounds are typically higher inside residential homes than outside,[1,13] which suggests that the source of indoor emissions has a stronger influence than the infiltration of outdoor air. Furthermore, the concentration of water-soluble organic compounds inside residential areas has also been found to be, on average, 15 times higher than immediately outside.[5] This then further supports that a majority of indoor pollutants are emitted or formed within indoor environments. One significant indoor emission source is human activity in the household, such as cooking, frying, baking, and using cleaning and personal care products.[1,3] In addition, human metabolism and off-gassing of building materials and furnishings are also considered as direct indoor emission sources.[1,3] The amount and diversity of indoor pollutants is large due to the different human activities and materials, and some of the organic compounds that have been identified in indoor air from direct sources are summarized in Table 1.1.

### 1.1.1 Pollutants Formed via Surface Chemistry

Not only are indoor pollutants directly emitted from sources, but chemical reactions that occur in the gas-phase or on indoor surfaces can form alternative products, which also influences the composition of indoor air.[1] Examples of some reaction products identified in indoor air are

summarized in Table 1.2. Surface chemistry is crucial to study because these reactions can have a larger impact than gas-phase processes within indoor environments.[9] In addition, indoor environments have a high surface area-to-volume ratio of 2.9 – 4.6 $m^2 m^{-3}$.[1,2] Gas-phase reactions must occur faster than the air exchange rate in order to influence the indoor chemical composition, but they tend to react too slowly and cannot compete with air exchange.[9] However, previous studies demonstrated that surface conversion reaction rates occur faster than gas-phase reaction rates. Reactions between ozone and alpha-terpineol coated on various indoor surfaces had reaction rates 1 – 5 times greater than the gas-phase reaction rate,[14] and the reaction rates between ozone and dihydromyrcenol coated on indoor surfaces was 20 – 100 times greater than the gas-phase reaction rate.[15] Therefore, surface reactions and processes are important components of indoor chemistry.

Indoor environments encompass a wide range of surfaces, including window, carpet, building materials, wall cavities, furniture, paint, skin, hair, and clothing.[10] The diversity of surfaces found in indoor environments increases the multitude of chemical reaction that can occur in indoor environments. In addition, the formation of secondary products from surface chemistry will vary depending on the indoor conditions, such as relative humidity, temperature, pH, and light. Interfacial chemistry can occur readily through several of the following mechanisms: oxidative reactions, sorption, and acid-base chemistry.[1] Reactions between ozone and various indoor surfaces and compounds on these surfaces have been researched heavily, and it has been concluded that these oxidative reactions can reduce indoor ozone concentrations by a two 10-fold and, subsequently, increase the level of ozone reaction products.[2] Secondary organic aerosols, free radicals, volatile carbonyl compounds, carcinogens, and irritants are some of the products generated by the oxidation of organic matter on indoor surfaces.[2] However, there is a

lack of knowledge on the molecular understanding of surface speciation, surface-adsorbate interactions, and the effect of pH on these interactions.

## 1.2 Consequences of Indoor Surface Chemistry

As indoor air pollutants are mostly sourced or formed from within, ventilation plays a major role in minimizing the concentrations of air pollutants. However, new buildings are being designed to become more airtight in order to lower energy consumption.[6] These designs tend to decrease the air exchange rate and result in higher levels of indoor air pollutants, so alternative air treatment technologies have been introduced into indoor environments in hopes to improve indoor air quality.[6]

### 1.2.1 Prevalence and Adversity of Titanium Dioxide on Indoor Surfaces

One of the alternative air treatment suggestions is to incorporate self-cleaning surfaces inside buildings that use photocatalytic paints based on titanium dioxide nanoparticles.[6] Titanium dioxide ($TiO_2$), which is also an additive in sunscreen and other cosmetic products,[8] is a photosensitizer and can activate radical reactions in the presence of light to eliminate gas-phase pollutants.[5] Briefly, when $TiO_2$ is irradiated by photons with $\lambda < 390$ nm, the absorption of light separates the charges.[6] The electron from $TiO_2$ may be transferred to $O_2$ molecules in the air, and this reduction reaction will produce the superoxide radical ion ($O_2^-$).[6] Simultaneously, an oxidation reaction occurs when the electron vacancy accepts an electron from water molecules, which generates hydroxyl radicals (OH).[6] The hydroxyl radical can react with organic compounds, which should decompose adsorbed molecules on $TiO_2$ surfaces.[6] Although some decomposition does occur, production of other harmful organic compounds, such as nitrous acid

(HONO), formaldehyde, and acetaldehyde, have been measured at high concentrations upon the irradiation of photocatalytic paints.[6]

### 1.2.2 Relationship between Titanium Dioxide and Carboxylic Acids

Besides being a source of injurious compounds in indoor environments, $TiO_2$ also selectively adsorbs carboxylic acids that, on average, have a concentration of 6.8 ppb in indoor environments.[4,7] While other adsorbates, such as alcohols, are present at much higher concentration levels, $TiO_2$ obtains a high affinity towards atmospheric carboxylic acids due to their strong bidentate binding.[7] Other small molecules, such as alcohols and amines, adsorb onto $TiO_2$ through monodentate binding, so they can desorb easily around room temperature; carboxylic acids, on the other hand, form two bonds to $TiO_2$ that allows them to be more stable on the substrate.[7] Carboxylic acids are important pollutants to study because the extended residence time of reactants on surfaces can increase the possibility for future conversions to occur.[2] In addition, they are considered as irritants for the eyes, skin, and mucous membranes and can cause harm to the optic nerve, brain, heart, and kidney.[4] Carboxylic acids also have been found to damage indoor facilities; for example, formic acid and acetic acid can corrode church organ pipes.[4] Concentrations of carboxylic acids increase when unsaturated compounds react with ozone in the gas-phase or on surfaces, and some are correlated to the presence of carbon dioxide.[4] In a university classroom study conducted by Liu et al., they distinguished 12 carboxylic acids associated with carbon dioxide,[4] so this relationship suggests that human occupants contribute significantly to the composition of indoor air, especially in densely populated spaces like classrooms, aircraft cabins, and office buildings.[1] Yet, to our knowledge, there is minimal research on how indoor chemistry is influenced by human emissions on

surfaces.[1] Two indoor-air relevant carboxylic acids that are sourced from humans are lactic acid and pyruvic acid.[4,5]

## 1.3 Effect of Dampness and pH in Indoor Environments

Two common conditions of indoor environments that have not been widely examined is dampness and change in pH levels. A substantial amount of residential homes and buildings – roughly 18 to 50% – in the United States of America are affected by dampness.[5] An area is considered "damp" when there is a presence of standing water, mold exposure, or water-damaged materials.[5] This circumstance can be caused by several factors, such as water leakage from pipes in buildings, water infiltration or flooding, and water vapor condensation on indoor surfaces from human activities.[5] Some indoor surfaces, like air conditioning coils and exterior windows, are only seasonally wet in the summer and winter, respectively, while other surfaces, like sinks and bathroom walls, are constantly cycling between being wet and dry.[5] Hygroscopic surfaces, such as glass, paint, wallboards, and clothing, can adsorb water vapor and create several monolayers of condensed water molecules where aqueous-phase reactions can take place.[1,5] Aqueous-phase chemistry in indoor environments can produce different products than gas-phase reactions, which will further alter the chemical composition of indoor air and affect human exposure in damp homes.[5]

Change in pH levels is important to study because acidity can influence the tendency for molecules to adsorb on or desorb off from indoor surfaces, especially in liquid water.[1,5] Indoor environments have been found to be within the pH range of 5 – 9 since carbon dioxide emitted from human occupants will create more acidic environments, while the usage of ammonia-based cleaning products can lead to more basic conditions.[5] The change in pH can affect the reactivity

and concentration of species on surfaces; thus, in order to achieve a better understanding on indoor chemistry, the effect of pH needs to be investigated as well.

## 1.4 Main Objective of Research

This thesis focuses on understanding the surface chemistry and adsorption kinetics of two indoor-relevant carboxylic acids that have been sourced from human occupants, lactic acid and pyruvic acid,[4,5] on titanium dioxide nanoparticles, which is a major component in paints and self-cleaning surfaces. These two carboxylic acids are both water-soluble organic gases, with Henry's law constants of 12,000 M $atm^{-1}$ and 310,000 M $atm^{-1}$,[5] respectively, so they can assimilate into the aqueous phase by being absorbed into the water layers that are on indoor surfaces; thus, these studies will be performed in the liquid phase. Additionally, as previously stated, environmental acidity can influence chemical reactions, so the effect of pH will be investigated within indoor relevance, specifically at pH 5 and 8.

This thesis will be focusing on answering the following scientific questions:

1. How do these water-soluble organic acids adsorb onto $TiO_2$ surfaces; if they adsorb, do these compounds weakly and reversibly adsorb (physisorption) or do they strongly and irreversibly adsorb (chemisorption)?
2. Can reactions between the surface bound molecular species occur and can these products desorb from the surface into the water phase with time?
3. Given the presence of carbon dioxide or ammonia in indoor environments, which can also partition into the water phase and change the pH of the water film, how does pH affect the adsorption process and surface coverage?

Chapter 3 discusses the surface chemistry of lactic acid and pyruvic acid on titanium dioxide surfaces, as a function of pH, which was studied with the use of attenuated total reflectance-Fourier transform infrared spectroscopy (ATR-FTIR). Chapter 4 discusses the adsorption kinetics of lactic acid and pyruvic acid on titanium dioxide surfaces, as a function of pH, which was studied with the use of ATR-FTIR coupled with quartz crystal microbalance with dissipation (QCM-D). Finally, chapter 5 summarizes the findings of the previous two chapters and outlines future studies.

## 1.5 Tables

**Table 1.1.** Organic compounds identified inside residential areas and their source(s) of emission.

| Compound | Source(s) |
|---|---|
| Methanol | Wood Products[3] |
| Acetic Acid | Plant Material, Household Products[3] |
| 2-Propenal | Cooking, Building Products[3] |
| 2-Methylpropane | Propellant, Refrigerating Agent[3] |
| Isoprene | Building Occupants, Plants[3,5] |
| Furfural | Wood Products, Cooking[3] |
| Dimethylformamide | Leather Products[3] |
| Lactic Acid | Building Occupants[4,5] |
| Formaldehyde | Fireplace[5] |
| Acetaldehyde | Cooking[5] |
| Limonene | Cleaning Products[5] |

**Table 1.2.** Reaction products formed in the gas-phase or on indoor surfaces that have been identified inside residential areas and their source of emission.

| Compound | Source |
|---|---|
| Formaldehyde | Irradiation Product of Photocatalytic Paints[6] |
| Nitrous Acid (HONO) | Irradiation Product of Photocatalytic Paints[6] |
| Carvone | Oxidation Product of Limonene[10] |
| 2-Nonenal | Oxidation Product of Carpet Components[10] |
| Propanoic Acid | Degradation Product of Fatty Acids[3] |
| Butanal | Degradation Product of Fatty Acids[3] |

## 1.6 References


1. Nazaroff, W. W.; Goldstein, A. H. Indoor chemistry: research opportunities and challenges. *Indoor Air.* **2015**, *25*, 357-361.

2. Morrison, G. Interfacial Chemistry in Indoor Environments. *Environ. Sci. Technol*. **2008**, *42*, 3495-3499.

3. Salthammer, T. Very volatile organic compounds: an understudied class of indoor air pollutants. *Indoor Air*. **2016**, *26*, 25-38.

4. Liu, S.; Thompson, S. L.; Stark, H.; Ziemann, P. J.; Jimenez, J. L. Gas-Phase Carboxylic Acids in a University Classroom: Abundance, Variability, and Sources. *Environ. Sci. Technol*. **2017**, *51*, 5454-5463.

5. Duncan, S. M.; Sexton, K. G.; Turpin, B. J. Oxygenated VOCs, aqueous chemistry, and potential impacts on residential indoor air composition. *Indoor Air*. **2018**, *28*, 198-212.

6. Gandolfo, A.; Marque, S.; Temime-Roussel, B.; Gemayel, R.; Wortham, H.; Truffier-Boutry, D.; Bartolomei, V.; Gligorovski, S. Unexpectedly High Levels of Organic Compounds Released by Indoor Photocatalytic Paints. *Environ. Sci. Technol*. **2018**, *52*, 11328-11337.

7. Balajka, J.; Hines, M. A.; DeBenedetti, W. J. I.; Komora, M.; Pavelec, J.; Schmid, M.; Diebold, U. High-affinity adsorption leads to molecularly ordered interfaces on $TiO_2$ in air and solution. *Science*. **2018**, *361*, 786-789.

8. Jayalath, S.; Wu, H.; Larsen, S. C.; Grassian, V. H. Surface Adsorption of Suwannee River Humic Acid on $TiO_2$ Nanoparticles: A Study of pH and Particle Size. *Langmuir*. **2018**, *34*, 3136-3145.

9. Weschler, C. J. Chemistry in indoor environments: 20 years of research. *Indoor Air*. **2011**, *21*, 205-218.

10. Weschler, C. J.; Wells, J. R.; Poppendieck, D.; Hubbard, H.; Pearce, T. A. Workgroup Report: Indoor Chemistry and Health. *Environ. Health Perspect*. **2006**, *114*, 442-446.

11. Zhu, L.; Jacob, D. J.; Keutsch, F. N.; Mickley, L. J.; Scheffe, R.; Strum, M.; Abad, G. G.; Chance, K.; Yang, K.; Rappengluck, B.; Millet, D. B.; Baasandorj, M.; Jaegle, L.; Shah, V. Formaldehyde (HCHO) As a Hazardous Air Pollutant: Mapping Surface Air Concentrations from Satellite and Inferring Cancer Risks in the United States. *Environ. Sci. Technol*. **2017**, *51*, 5650-5657.

12. Khoder, M. I.; Shakour, A. A.; Farag, S. A.; Abdel Hameed, A. A. Indoor and outdoor formaldehyde concentrations in homes in residential areas in Greater Cairo. J. *Environ. Monit*. **2000**, *2*, 123-126.

13. Adgate, J. L.; Church, T. R.; Ryan, A. D.; Ramachandran, G.; Fredrickson, A. L.; Stock, T. H.; Morandi, M. T.; Sexton, K. Outdoor, Indoor, and Personal Exposure to VOCs in Children. *Environ. Health Perspect*. **2004**, *112*, 1386-1392.

14. Shu, S.; Morrison, G. C. Surface Reaction Rate and Probability of Ozone and Alpha-Terpineol on Glass, Polyvinyl Chloride, and Latex Paint Surfaces. *Environ. Sci. Technol*. **2011**, *45*, 4285-4292.

15. Shu, S.; Morrison, G. C. Rate and reaction probability of the surface reaction between ozone and dihydromyrcenol measured in a bench scale reactor and a room-sized chamber. *Atmospheric Environment*. **2012**, *47*, 421-427.

# Chapter 2 Experimental Methods and Materials

This chapter provides an overview of the experimental methods used in these studies along with the materials purchased including solvents, reagents, and nanomaterials. For most of the research, two analytical techniques were used to study the surface chemistry and adsorption kinetics of lactic acid and pyruvic acid on $TiO_2$ nanoparticle surfaces: Attenuated Total Reflectance-Fourier Transform Infrared Spectroscopy (ATR-FTIR) and Quartz Crystal Microbalance with Dissipation (QCM-D).

## 2.1 Chemical Reagents and Nanomaterials

The chemical reagents used in this thesis were D,L-Lactic Acid (Acros, 85%) and Pyruvic Acid (Sigma Aldrich, 98%). Lactic acid was used as received from the source bottle, while pyruvic acid was distilled under reduced pressure at 100 °C every two months to remove impurities, including zymonic acid.[12] The pH of the solutions was adjusted with the use of 1 N NaOH (Fisher Scientific ACS plus) and 1 N HCl (Fisher Scientific ACS plus).

The $TiO_2$ nanoparticles used for ATR-FTIR spectroscopy studies were purchased from Sigma Aldrich (SKU-718467). Transmission electron microscopy (TEM) determined the primary nanoparticle size is 22 ± 1 nm, and BET (Brunauer, Emmett, and Teller) analysis determined the surface area for $TiO_2$ is 50 ± 8 $m^2/g$.[10] The phase state for these nanoparticle was determined to be 86% anatase and 14% rutile from the X-ray diffraction (XRD) pattern.[10] The isoelectric point for $TiO_2$ was also experimentally determined to be pH 6.5,[10] which is consistent with literature reported values of about pH 7.0.[11]

## 2.2 Attenuated Total Reflectance-Fourier Transform Infrared Spectroscopy

### 2.2.1 Brief Background of ATR-FTIR Spectroscopy

Infrared spectroscopy (IR) is a well-established analytical technique that determines the structures of molecules through absorption bands that are characteristic of vibrational energy transitions.[1] In order for a molecule to be IR active, there must be a change in dipole moment in the molecule when it absorbs infrared light.[1] Molecules that are IR active absorb specific wavelengths of infrared light, and this will excite the vibrational energy levels from ground state to excited state.[1] The vibrational energy gap is determined by the involved atoms and their bond strength, which will also determine the frequency of the absorption band. Therefore, each functional group or molecular bond has an individual absorption frequency, so molecular structures can be established.

ATR-FTIR, an IR technique commonly used to study the surface chemistry at a solid-liquid interface, is based on the principle of total internal reflection of infrared light at the boundary between two media.[1,2] Generally, the sample of interest is placed on an internal reflection element (IRE).[2] The infrared light generated from the spectrometer, at an angle of incidence greater than the critical angle, undergoes total internal reflection when it passes through the IRE.[2] At each internal reflection point on the IRE, an evanescent wave is produced, and the sample of interest on the IRE then absorbs the infrared light from the evanescent wave that has a specific depth of penetration.[2] After multiple reflections, the infrared light, which has specific frequencies adsorbed by the sample, eventually exits the IRE and enters the detector. This basic principle on ATR-FTIR is illustrated in Figure 2.1.

Penetration depth ($d_P$) is the required distance to decrease the electric field amplitude to $e^{-1}$ of its value at the surface, which is given by the following equation:

$$d_P = \frac{\lambda}{2\pi n_1 \sqrt{[sin^2\,\theta - (n_2/n_1)^2]}} \qquad \text{(Eq2.1)}$$

where $\lambda$ is the incidence wavelength, $n_1$ is the index of refraction of the IRE, $n_2$ is the index of refraction of the sample of interest in contact with the IRE, and $\theta$ is the angle of incidence.[1] For amorphous material transmitting infrared (AMTIR) crystal, which was used in this thesis, the penetration depth is 1.46 μm.[1]

The absorption of infrared light ($A$) is proportional to the concentration and effective path length, as shown in the modified Beer-Lambert law:

$$A = \varepsilon c b' \qquad \text{(Eq2.2)}$$

where ε is the molar absorptivity coefficient, $c$ is the concentration, and $b'$ is the effective path length.[2] Effective path length equals to the number of reflections of the IR beam ($N$) times the depth of penetration ($b' = Nd_P$).[2]

ATR-FTIR is an excellent technique to study surface adsorption on nanomaterials in either a qualitative or quantitative way.[1] It can be used for *in-situ* characterization of liquid-surface interfaces, such as structural changes of ligands on surfaces, or for determining quantitative information, such as kinetic adsorption parameters.[1]

## 2.2.2 Experimental Procedures and Methods Used for ATR-FTIR Spectroscopy Experiments

For both surface chemistry and adsorption kinetic studies, a 500 µl horizontal ATR flow cell with an AMTIR window (Pike Technologies Inc.) was used in a Nicolet iS 10 FTIR spectrometer equipped with an MCT-A detector. An evenly coated $TiO_2$ film was placed onto the AMTIR crystal. The $TiO_2$ film was prepared by sonicating a suspension of $TiO_2$ (2 mg in 1 mL of Milli-Q water) for 20 minutes, drop-casting the suspension onto the crystal, and drying it overnight. All AMTIR-FTIR spectra were collected in the AMTIR window range of 750 to 4000 $cm^{-1}$ with a resolution of 4 $cm^{-1}$. Figure 2.2 illustrates the experimental set-up.

### 2.2.2.1 Surface Chemistry Studies

For surface chemistry studies, solutions of 5 mM lactic acid were prepared at three pH values: unadjusted pH of 3 and adjusted pH values of 5 and 8 for indoor relevance. Similarly, solutions of 5 mM pyruvic acid were also prepared at three pH values: unadjusted pH of 2.6 and adjusted pH values of 5 and 8 for indoor relevance. $TiO_2$ surface was flushed with Milli-Q $H_2O$ (adjusted to pH of interest) for 30 minutes to remove any loosely bound nanoparticles prior to flowing 5 mM lactic acid or 5 mM pyruvic acid solution (at pH of interest) for 30 minutes. Immediately afterwards, Milli-Q $H_2O$ (adjusted to pH of interest) was flowed over the $TiO_2$ surface for 30 minutes for desorption. Adsorption and desorption spectra were collected every five minutes, and all solutions flowed over the $TiO_2$ film with a flow rate of 0.8 mL $min^{-1}$. Solution phase spectra were collected for 100 mM lactic acid solutions adjusted to pH values of 3, 5, and 8, and 100 mM pyruvic acid solutions adjusted to pH values of 2.6, 5, and 8.

#### 2.2.2.2 Adsorption Kinetics Studies

For adsorption kinetic studies, only indoor-relevant pHs were examined, so the 5 mM lactic acid and 5 mM pyruvic acid solutions were adjusted to pH 5 and 8. $TiO_2$ surface was first flushed with Milli-Q $H_2O$ (adjusted to pH of interest) for 30 minutes. Afterwards, 5 mM lactic acid or 5 mM pyruvic acid solution (at the pH of interest) was flowed over the surface with a flow rate of 0.8 mL $min^{-1}$ until equilibration was achieved. Equilibrium was determined to be achieved when peak intensities did not change over time. Lastly, desorption with Milli-Q $H_2O$ (adjusted to pH of interest) followed until equilibration was achieved as well. Spectra were collected every 30 seconds to monitor the adsorption and desorption process.

## 2.3 Quartz Crystal Microbalance with Dissipation

### 2.3.1 Brief Background of QCM-D Technique

QCM-D has developed over the last two decades to become a powerful analytical technique due to its ability to provide *in-situ* characterization of molecular interactions at the liquid and solid interface.[3,4] With QCM-D, the amount of mass of adsorbed molecules on the surface can be determined by measuring the changes in quartz crystal frequency. Therefore, by coupling ATR-FTIR with QCM-D, the qualitative observations from the ATR-FTIR studies can be verified and supported with quantitative mass information obtained from QCM-D.

QCM-D involves a crystal, which is a thin piezoelectric quartz disc that is sandwiched between two electrodes, as shown in Figure 2.3a, and it oscillates at its resonance frequency when an alternating current voltage is applied across the pair of electrodes.[3] The crystals used in QCM-D are AT-cut quartz crystals, and this cut of crystal vibrates in the thickness-shear mode, where the top and bottom surfaces move tangentially in an antiparallel fashion, as shown in

Figure 2.3b.[4] In addition, the crystal can be excited to resonate at higher odd harmonics. The lowest resonance frequency that can be excited is the fundamental harmonic (n = 1), while a set of overtone harmonics (n = 3, 5, 7, ect.) resonates at odd multiples of the fundamental frequency.[7] For example, for a 5 MHz AT-cut QCM crystal, the overtones (n = 3, 5, 7) will resonate at 15 MHz, 25 MHz, and 35 MHz, respectively.[7] The advantage of multi-harmonic measurements will be discussed later in this chapter.

QCM-D uses a ring-down method, and this technique allows the instrument to simultaneously measure the changes of two parameters per overtone: resonance frequency and energy dissipation.[4] Resonance frequency depends on the total mass of the oscillating crystal and surface adhering film.[3] If any adsorption on the crystal occurs, the frequency decreases. For thin rigid films, the change in frequency ($\Delta f_n$) is directly proportional with the change in mass ($\Delta m_f$), as derived by the Sauerbrey equation:

$$\Delta f_n = -\frac{n}{C}\Delta m_f \qquad \text{(Eq2.3)}$$

where $n$ is the harmonic overtone and $C$ is the mass sensitivity constant, which is 18 ng cm$^{-2}$ Hz$^{-1}$ for 5 MHz crystals.[3,4]

Dissipation ($D$) is defined as the sum of energy losses in the system per oscillation cycle:

$$D = \frac{E_{dissipation}}{2\pi E_{stored}} \qquad \text{(Eq2.4)}$$

where $E_{dissipation}$ is the energy dissipated per oscillation, and $E_{stored}$ is the energy stored in the oscillating system.[5] In the ring-down method, the external driving voltage is periodically switched off, and the oscillation will freely decay, in which the time of oscillation decay is monitored.[3,4] Change in dissipation provides *in-situ* structural information on the viscoelastic

properties of the adsorbed film, determining whether the adsorbed film is rigid or soft.[3] If a molecule adsorbs rigidly onto the surface, the molecule will follow the oscillation of the crystal. Consequently, the rigid film will not dampen the crystal's oscillation, and the increase in dissipation will be small.[8] On the other hand, a soft film, which exhibits more viscoelastic properties, will deform and not couple well to the oscillation of the crystal. The soft film will dampen the crystal's oscillation, and the increase in dissipation will be large.[8] Figure 2.4 depicts the difference in frequency and dissipation change due to the adsorption of rigid and soft films in an example QCM-D data set.

As mentioned earlier, QCM-D can collect multi-harmonic measurements, and this is advantageous because it provides more information when characterizing the adhered film and confirms its viscoelastic properties.[7] If the change in resonance frequency and dissipation is similar or overlapping for separate harmonics, it confirms that the film is truly rigid and the application of the Sauerbrey equation is valid. As stated earlier, in order for the Sauerbrey equation to be applied for mass change calculations, the film on the crystal must be thin and rigidly attached. Therefore, as long as the dissipation does not exceed 2 ppm, the Sauerbrey equation can be successfully applied.[6]

### 2.3.2 Experimental Procedure and Method Used for QCM-D Experiments

The adsorption and desorption behavior of lactic acid and pyruvic acid on $TiO_2$ was examined complementarily by a quartz crystal microbalance with dissipation (Qsense Pro, Biolin Scientific) and commercially custom-made $TiO_2$ coated 5 MHz AT-cut quartz crystals (QSX 999, Biolin Scientific). A picture of the QCM-D used is shown in Figure 2.5. Shifts in frequency and energy dissipation were collected over time as 20 mM lactic acid or 20 mM

pyruvic acid solutions (adjusted to pH of interest) adsorbed on $TiO_2$ coated quartz crystals. For QCM-D studies, only indoor-relevant pHs were examined, so the 20 mM lactic acid and 20 mM pyruvic acid solutions were adjusted to pH 5 and 8.

A baseline was first collected for 15 minutes with Milli-Q $H_2O$. Then, 20 mM lactic acid or 20 mM pyruvic acid solution (adjusted to pH of interest) flowed over the $TiO_2$ crystal at a flow rate of 50 μL $min^{-1}$ for 60 minutes. Subsequently, the flow was stopped with the solution over the crystal for 30 minutes to achieve equilibrium. Equilibrium was established in order to clearly read the final change in resonance frequency and dissipation. Lastly, Milli-Q $H_2O$ was re-introduced for desorption, by flowing it over the $TiO_2$ coated crystal at a flow rate of 50 μL $min^{-1}$ for 60 minutes and then stopping it for 30 minutes to reach equilibrium. Harmonic overtones (n = 3, 5, 7, 9, and 11) were monitored for all measurements.

## 2.4 Figures

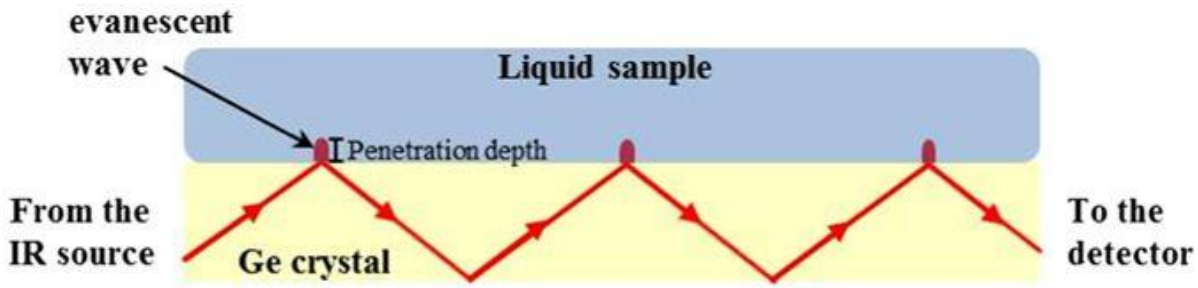


**Figure 2.1.** Pictorial representation of the reflection pathway of infrared radiation through an ATR crystal and sample. Image reprinted from Minnes, R.; Nissinmann, M.; Maizels, Y.; Gerlitz, G.; Katzir, A.; Raichlin, Y. Using Attenuated Total Reflection-Fourier Transform Infra-Red (ATR-FTIR) spectroscopy to distinguish between melanoma cells with a different metastatic potential. *Scientific Reports*. [Online] **2017**, *7*, 4381 https://www.nature.com/articles/s41598-017-04678-6 (accessed April 28, 2019).

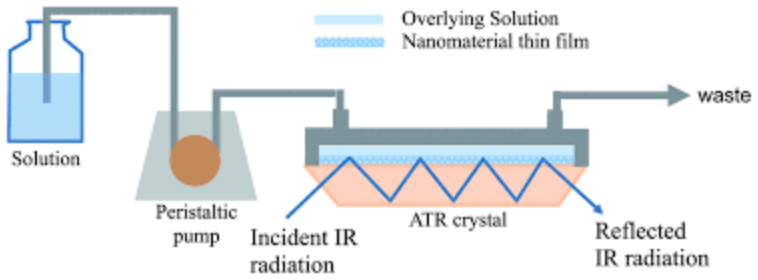


**Figure 2.2.** ATR-FTIR experimental set-up to study surface chemistry and adsorption kinetics of lactic acid and pyruvic acid on $TiO_2$ nanoparticle surface, as a function of pH, in the aqueous-phase. Image reprinted from Mudunkotuwa, I. A.; Minshid, A. A.; Grassian, V. H. ATR-FTIR spectroscopy as a tool to probe surface adsorption on nanoparticles at the liquid-solid interface in environmentally and biologically relevant media. *Analyst*. **2014**, *139*, 870-881.

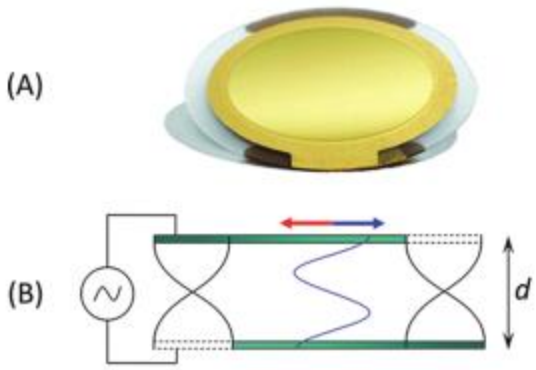


**Figure 2.3.** (A) 5 MHz AT-cut quartz crystal supplied from Q-Sense. (B) Side view of oscillating quartz crystal when alternative current voltage is applied. The black waves at the edge of the crystal illustrate the fundamental frequency, and the blue wave in the middle of the crystal illustrate the third harmonic overtone. Image reprinted from Reviakine, I.; Johannsmann, D.; Richter, R. P. Hearing What You Cannot See and Visualizing What You Hear: Interpreting Quartz Crystal Microbalance Data from Solvated Interfaces. *Anal. Chem*. **2011**, *83*, 8838-8848.

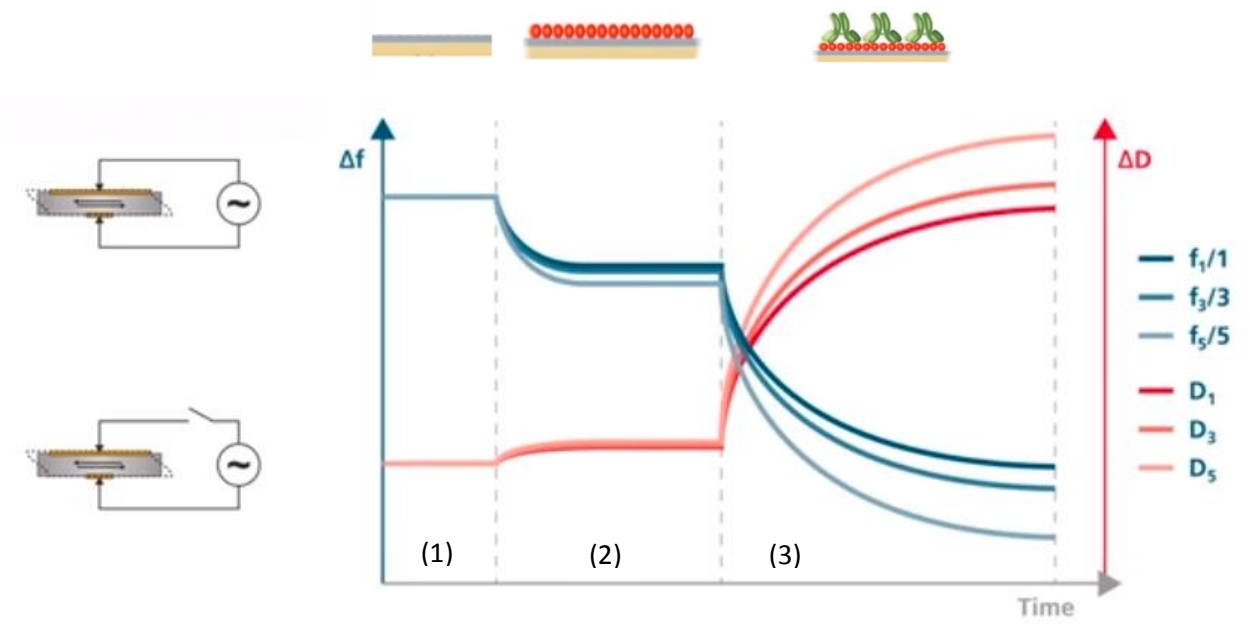


**Figure 2.4.** Example data set depicting the change in resonance frequency (blue) and dissipation (red) over time for three harmonics (n = 1, 3, 5) during adsorption process. In step 1, the background of the crystal is measured. In step 2, a sample solution (represented by the red spheres) is introduced, and a decrease in frequency and increase in dissipation is observed due to adsorption taking place. This sample is adsorbing rigidly to the surface as the dissipation change is quite small. In step 3, another sample solution (represented by the elongated green ovals) is introduced, and a large decrease in frequency and increase in dissipation is observed. Additionally, the different harmonics are beginning to spread apart, which signifies that this sample is more viscoelastic than the previous sample. Image reprinted from NanoScience Instruments. The QCM-D Technology: How to Perform Experiments & Analyze Data. https://www.nanoscience.com/qsense-technique-overview/ (accessed April 28, 2019).

**Figure 2.5.** QCM-D experiments were performed with the fully automated Qsense Pro manufactured by Biolin Scientific. Image reprinted from NanoScience Instruments. The QCM-D Technology: How to Perform Experiments & Analyze Data. https://www.nanoscience.com/qsense-technique-overview/ (accessed April 28, 2019).

## 2.5 References


1. Mudunkotuwa, I. A.; Minshid, A. A.; Grassian, V. H. ATR-FTIR spectroscopy as a tool to probe surface adsorption on nanoparticles at the liquid-solid interface in environmentally and biologically relevant media. *Analyst*. **2014**, *139*, 870-881.

2. Schuttlefield, J. D.; Grassian, V. H. ATR-FTIR Spectroscopy in the Undergraduate Chemistry Laboratory. Part I: Fundamentals and Examples. *J. Chem. Educ*. **2008**, *85*, 279-281.

3. Jaiswal, A.; Smoukov, S.; Poggi, M.; Grzybowski, B. Quartz Crystal Microbalance with Dissipation Monitoring (QCM-D): Real-Time Characterization of Nano-Scale Interactions at Surfaces. *NSTI-Nanotech.* **2008**, *1*, 855-858.

4. Reviakine, I.; Johannsmann, D.; Richter, R. P. Hearing What You Cannot See and Visualizing What You Hear: Interpreting Quartz Crystal Microbalance Data from Solvated Interfaces. *Anal. Chem*. **2011**, *83*, 8838-8848.

5. Biolin Scientific. Quartz Crystal Microbalance with Dissipation (QCM-D): Measurements. https://www.biolinscientific.com/measurements/qcm-d (accessed April 28, 2019).

6. Vogt, B. D.; Lin, E. K.; Wu, W.; White, C. C. Effect of Film Thickness on the Validity of the Sauerbrey Equation for Hydrated Polyelectrolyte Films. *J. Phys. Chem. B*. **2004**, *108*, 12685-126900.

7. Edvardsson, M. Biolin Scientific Blog: Why are overtones important in QCM? https://blog.biolinscientific.com/why-are-overtones-important-in-qcm (accessed April 28, 2019).

8. NanoScience Instruments. The QCM-D Technology: How to Perform Experiments & Analyze Data. https://www.nanoscience.com/qsense-technique-overview/ (accessed April 28, 2019).

9. Minnes, R.; Nissinmann, M.; Maizels, Y.; Gerlitz, G.; Katzir, A.; Raichlin, Y. Using Attenuated Total Reflection-Fourier Transform Infra-Red (ATR-FTIR) spectroscopy to distinguish between melanoma cells with a different metastatic potential. *Scientific Reports*. [Online] **2017**, *7*, 4381 https://www.nature.com/articles/s41598-017-04678-6 (accessed April 28, 2019).

10. Givens, B. E.; Xu, Z.; Fiegel, J.; Grassian, V. H. Bovine serum albumin adsorption on $SiO_2$ and $TiO_2$ nanoparticle surfaces at circumneutral and acidic pH: A tale of two nano-bio surface interactions. *Journal of Colloid and Interface Science*. **2017**, *493*, 334-341.

11. Kosmulski, M. pH-dependent surface charging and points of zero charge. *J Colloid Interface Sci*. **2006**, *298*, 730-741.

12. Reed Harris, A. E.; Pajunoja, A.; Cazaunau, M.; Gratien, A.; Pangui, E.; Monod, A.; Griffith, E. C.; Virtanen, A.; Doussin, J. F.; Vaida, V. Multiphase Photochemistry of Pyruvic Acid under Atmospheric Conditions. *J. Phys. Chem. A.* **2017**, *121*, 3327-3339.

# Chapter 3 Surface Chemistry of Lactic Acid and Pyruvic Acid on $TiO_2$ Nanoparticles: A Study of pH Effects

## 3.1 Lactic Acid

Lactic acid, $CH_3CH(OH)COOH$, has been identified as one of the most abundant carboxylic acids present in indoor environments, with an indoor concentration of 4700 ppt, and is sourced mainly from human perspiration.[1,2] Table 3.1 and Figure 3.1 show the structure of lactic acid and the fraction of lactic acid and lactate species in solution as a function of pH, respectively. The fraction of species – within the pH range of 1 to 11 – was determined from the following equilibrium equations:

$$Fraction\ of\ Lactic\ Acid = \frac{[H^+]}{[H^+]+K_a} \qquad \text{(Eq3.1) and}$$

$$Fraction\ of\ Lactate = \frac{K_a}{[H^+]+K_a} \qquad \text{(Eq3.2),}$$

where Ka is the dissociation constant, which can be determined from pKa (pKa = -log(Ka) is 3.86), and $[H^+]$ is the proton ion concentration, which is calculated at each pH (pH = -log$[H^+]$). As pH increases, the fraction of lactic acid decreases while the fraction of lactate ($CH_3CH(OH)COO^-$) increases due to the deprotonation of lactic acid. Based on Figure 3.1, major fraction of lactic acid species in solution should be neutral, neutral/anionic, and anionic in the pH ranges of < 3.0, between 3.0 and 5.0, and > 5.0, respectively.

For this study, lactic acid was investigated at three different pH values: pH 3, 5, and 8. Figure 3.2 presents the solution phase spectra for lactic acid at these pH values. The peak assignments observed in the solution phase of lactic acid at pH 3 are listed in Table 3.2(a), and

the peaks assignments observed in solution phase spectra of lactic acid at pH 5 and 8 are listed in Table 3.3. The band at 1728 $cm^{-1}$ is assigned to the stretching vibration of C=O in the protonated carboxylic group (COOH). As pH increases, the intensity of this band decreases due to the deprotonation of the carboxylic group in lactic acid. Due to the deprotonation, intense peaks are observed at 1578 and 1414 $cm^{-1}$ for lactic acid solutions at pH 5 and 8, which are associated with the asymmetric and symmetric stretching vibrations of deprotonated carboxylic group ($COO^-$), respectively. The lactic acid solution spectra for pH 3 also contains the peaks associated with the asymmetric and symmetric stretching vibrations of $COO^-$ at 1587 and 1410 $cm^{-1}$, respectively, but the intensity of these peaks are much smaller than that for solutions at higher pH. These peaks signify that both lactic acid and lactate are present in solution at pH 3, and this is expected because neutral and anionic species should be observed between pH 3.0 and 5.0, as shown in Figure 3.1. In addition, the observed trend that the amount of deprotonated lactic acid increases as solution pH increases also agrees with the calculated speciation curve in Figure 3.1. Based on the calculated speciation, it is expected that lactic acid should be fully deprotonated at pH 8. However, this is not observed in the experimental solution spectrum collected at pH 8 since the peak associated with C=O stretching vibration is still present at 1736 $cm^{-1}$, as shown in Figure 3.2. Ube et al. (2017) also observed this discrepancy in their transmission IR absorbance spectra of aqueous lactic acid solutions at different pH values. For that study, lactic acid solutions ranged from pH 2.44 to 11.59, and full deprotonation of lactic acid was not observed experimentally until pH 11.59.[3] Thus, this previous study is in agreement with our experimental result that lactic acid is not fully deprotonated in pH 8 solution, which could be caused by the presence of impurities in lactic acid.

### 3.1.1 Lactic Acid Adsorption on $TiO_2$ Nanoparticles as *f*(pH)

A previous study on the adsorption of gas-phase lactic acid on $TiO_2$ proposes that lactate ($CH_3CH(OH)COO^-$) is formed by the deprotonation of carboxylic acid group.[4] Figure 3.3 compares the solution phase and adsorption spectra of lactic acid at pH 3 on $TiO_2$, and the peak assignments for the surface adsorption spectrum of lactic acid at pH 3 are listed in Table 3.2(b). The bands at 1738, 1624, and 1385 $cm^{-1}$ on the adsorption spectrum have been assigned, respectively, as the stretching vibration of C=O, asymmetric stretching vibration of $COO^-$, and symmetric stretching vibration of $COO^-$. Upon adsorption, peak intensity at 1738 $cm^{-1}$ decreases while the peak intensity at 1624 and 1385 $cm^{-1}$ increases, which signifies that further lactic acid does undergo deprotonation when adsorbed on $TiO_2$. In addition, there is a decrease in intensity for the band at 1223 $cm^{-1}$, and this band is associated with the bending frequencies of C-OH in the carboxylic group. The decrease in this band additionally suggests that there is deprotonation of COOH group. Since lactate forms upon adsorption on $TiO_2$, lactic acid can be deprotonated by the surface hydroxyl groups. When lactic acid adsorbs onto $TiO_2$ surface, a shift in wavenumbers occurs, as shown in Figure 3.3. Peaks associated with the asymmetric and symmetric stretching vibrations of $COO^-$ shift from 1587 to 1624 $cm^{-1}$ and 1410 to 1385 $cm^{-1}$, respectively, and these peak shifts are likely due to the interactions between the oxygen atoms of $COO^-$ and Lewis acid sites ($Ti^{4+}$) on $TiO_2$ surface.[4]

Figure 3.4 compares the solution phase spectra and adsorption spectra of lactic acid at pH 5 and 8, and the adsorption mechanism for lactic acid at pH 3 on $TiO_2$ is also observed for lactic acid at pH 5 and 8. Upon adsorption of lactic acid at pH 5, the band associated with C=O stretching vibration at 1733 $cm^{-1}$ decreases in intensity, and the bands associated with the asymmetric and symmetric stretching vibrations of $COO^-$ at 1618 and 1390 $cm^{-1}$, respectively,

increase in intensity. This same trend is observed when lactic acid at pH 8 adsorbs on $TiO_2$ surface due to the decrease in C=O stretching vibration at 1736 $cm^{-1}$ and increase in asymmetric and symmetric stretching vibrations of $COO^-$ at 1620 and 1392 $cm^{-1}$, respectively. Therefore, for lactic acid solutions between pH 3 and 8, further deprotonation occurs on the surface and lactate is formed. The proposed reaction for the deprotonation of lactic acid by surface hydroxyl groups is shown below:

$$Ti\text{-}OH + CH_3CH(OH)COOH \rightarrow CH_3CH(OH)COO\text{-}Ti + H_2O \qquad (Eq3.3)$$

### 3.1.2 Adsorption Reversibility and Binding Mode

In order to address the reversibility of the adsorption of lactic acid on $TiO_2$, the surface was flushed with Milli-Q water at the given pH of the lactic acid solution. If adsorption is reversible, the lactate absorption bands should decrease in intensity completely after desorption. Figure 3.5 shows the spectra collected after desorption for the three pH values. Although there is an overall decrease in peak intensities, lactate still remains on the surface after desorption for all three pH values, which concludes that much of the adsorbed lactic acid stays on the surface and the adsorption process is irreversible. The irreversibility of lactic acid adsorption is not surprising as previous studies have shown that adsorption of other organic acids on $TiO_2$, such as citric acid and humic acid, is irreversible as well.[5,6]

For carboxylate species, the type of binding occurring on the surface can be determined by the difference in the asymmetric and symmetric stretching vibrations of $COO^-$.[6] When a carboxylate binds to a single surface ion through one of the oxygen atoms, this coordination mode is monodentate, and the frequency difference for monodentate binding is roughly between 300 and 500 $cm^{-1}$.[6] On the other hand, when a carboxylate binds to two neighboring surface ions

through both oxygen atoms, this coordination mode is bidentate bridging, and the frequency difference for bidentate bridging is roughly between 150 and 260 $cm^{-1}$.[6-8] The frequency differences for lactate on $TiO_2$ surface at pH 3, 5, and 8 are 239, 228, and 228 $cm^{-1}$, respectively, and these values suggest that lactate binds to $TiO_2$ via bidentate bridging at all three pH values. A schematic of the proposed binding mode for lactic acid on $TiO_2$ is illustrated in Figure 3.6.

### 3.1.3 Adsorption Intensity as *f*(pH)

Figure 3.7 shows the adsorption of lactic acid on $TiO_2$ nanoparticles with varying solution pH between 3.0 and 7.5. In order to qualitatively observe the amount of adsorption occurring on the surface as a function of pH, the peak intensity associated to the symmetric stretching vibration of $COO^-$ at around 1390 $cm^{-1}$, which is representative of lactate species, will be examined. This peak was preferred over the peak associated to the asymmetric stretching of lactate at 1624 $cm^{-1}$ because it will not have any contribution from the water adsorption band that is usually around 1637 $cm^{-1}$. The general trend of lactic acid adsorption on $TiO_2$ is that it decreases as solution pH increases. The isoelectric point of $TiO_2$ nanoparticles is pH 6.5, so for pH < 6.5, the surface charge is mostly positive while it is negative for pH > 6.5. In addition, according to the speciation diagram in Figure 3.1, major fraction of species in solution pH < 4 is lactic acid while it is lactate in solution pH > 4. Therefore, with increasing pH, the positive surface charge of $TiO_2$ nanoparticles decreases, and solution becomes dominantly negative as lactic acid species deprotonate. The repulsive electrostatic interactions between the negatively-charged $TiO_2$ nanoparticles and anions from the lactate molecules result in little adsorption; thus, the observed decreasing adsorption trend as pH increases is expected and is in good agreement with other literatures that previously studied the pH effect on the adsorption of other organic acids including citric acid and humic acid on $TiO_2$.[5,6]

## 3.2 Pyruvic Acid

Pyruvic acid, $CH_3COCOOH$, is another carboxylic acid identified in indoor environments that is sourced from human occupants, and it has an indoor concentration of 31 ppt.[1,2] Unlike lactic acid, pyruvic acid in water can hydrate to its geminal-diol, 2-2-dihydroxypropanoic acid ($CH_3C(OH)_2COOH$), and both forms are present in the solution phase.[9] For the remainder of this thesis, $CH_3COCOOH$ will be referred as the ketone species and $CH_3C(OH)_2COOH$ as the diol species. The fraction of ketone and diol species is known to be dependent on solution pH,[9] and since the pKa of ketone and diol species are 2.18 and 3.6, respectively,[9] the fraction of neutral ketone, anionic ketone, neutral diol, and anionic diol species will vary as a function of pH. Table 3.4 shows the structures of these four species and their percent fractions that were experimentally determined with nuclear magnetic resonance spectroscopy (NMR) over a pH range between 1.11 and 7.92. This NMR experiment was conducted by Man Luo, and her data confirms the pH dependence of pyruvic acid speciation in aqueous solution that has been observed in previous literature.[9] Major fraction of pyruvic acid molecules in solution are diol species when solution pH < 2.4, but as pH increases, fraction of ketone species increases where roughly 90% pyruvic acid molecules are in the ketone form by pH 5.

For this study, pyruvic acid was studied at three different pH values: pH 2.6, 5, and 8. In Figure 3.8, the solution phase spectra for pyruvic acid at these pH values are shown, and the change in pyruvic acid speciation as a function of pH is observed. The peak assignments for pyruvic acid in solution pH 2.6 are listed in Table 3.5(a), and the peak assignments for pyruvic acid in solution pH 5 and 8 are listed in Table 3.6. At pH 2.6, the band at 1734 $cm^{-1}$ is assigned to the stretching vibration of C=O in the carboxylic group (COOH), while the band at 1709 $cm^{-1}$ is assigned to the stretching vibration of C=O in the ketone group. Based on the NMR data in

Table 3.4, deprotonated pyruvic acid is expected to be present when pH > 2.0, and this is observed in the collected solution spectrum at pH 2.6 due to the presence of peaks at 1601 and 1394 $cm^{-1}$, which are associated with the asymmetric and symmetric stretching vibration of $COO^-$, respectively. In addition, pyruvic acid solution at pH 2.6 has peaks present at 1161 and 1105 $cm^{-1}$, which are associated with the stretching vibration of C-O in alcohol groups. Alcohol groups are only present in the diol species, so the presence of these peaks suggests that both ketone and diol species are in pH 2.6 solution. This observation is in good agreement with the percent fractions in Table 3.4 and previous literature.[9] As solution pH increases to pH 5 and 8, the band at 1734 $cm^{-1}$, which is associated with the C=O stretching vibration in COOH, disappears because pyruvic acid molecules have fully deprotonated. Due to the greater presence of pyruvate species, the intensity of peaks associated with the asymmetric and symmetric stretching vibrations of $COO^-$ at 1601 and 1394 $cm^{-1}$, respectively, increases. In addition, pyruvic acid solutions at pH 5 and 8 do not have peaks at 1161 and 1105 $cm^{-1}$, which are associated with the C-O stretching vibrations in alcohol groups, and thus, diol species are not present in solution phase at pH 5 and 8, which is expected based on the experimental data obtained from NMR in Table 3.4.

### 3.2.1 Pyruvic Acid Adsorption on $TiO_2$ Nanoparticles as *f*(pH)

A previous study on the adsorption of gas-phase pyruvic acid on $TiO_2$ proposes that deprotonation of pyruvic acid occurs upon adsorption.[10] Figure 3.9 compares the solution phase and adsorption spectra of pyruvic acid at pH 2.6 on $TiO_2$, and the peak assignments for surface adsorption spectrum at pH 2.6 are listed in Table 3.5(b). The bands at 1649 and 1385 $cm^{-1}$ on the adsorption spectrum have been assigned as the asymmetric and symmetric stretching vibration of $COO^-$, respectively. Upon adsorption, the peak intensity at these two peaks increases, and the

peak at 1734 $cm^{-1}$ in solution spectrum, which is associated with the stretching vibration of the carbonyl in carboxylic acid group, is not present in the adsorption spectrum. The growth of peaks associated with stretching vibrations of $COO^-$ and disappearance of the peak associated with C=O stretching of COOH signify that further deprotonation of pyruvic acid occurs when it adsorbs on $TiO_2$. In addition, there is a decrease in intensity for the band at 1281 $cm^{-1}$ upon adsorption, and this band is associated with the bending frequency of C-(OH) in the carboxylic group. The decrease in intensity for this peak additionally suggests that the carboxylic group deprotonates when pyruvic acid adsorbs on $TiO_2$, so similar to lactic acid, pyruvic acid can be deprotonated by the surface hydroxyl groups. The peaks associated to the asymmetric and symmetric stretching vibrations of $COO^-$ shift from 1601 to 1649 $cm^{-1}$ and 1394 to 1385 $cm^{-1}$, respectively, when pyruvic acid adsorbs on $TiO_2$ surface. These peak shifts are likely due to the interactions between the oxygen atoms in $COO^-$ and surface $Ti^{4+}$ ions, and they are in good agreement with the observations for lactic acid adsorption on $TiO_2$. The adsorption spectrum at pH 2.6 also suggests that both ketone and diol species are adsorbed on the surface due to the presence of peaks at 1709 and 1140 $cm^{-1}$, which are associated to the stretching vibration of C=O in ketone group and stretching vibration of C-O in alcohol group, respectively. The presence of both ketone and diol species on $TiO_2$ at pH 2.6 is not surprising as the NMR data in Table 3.4 shows that both species are roughly equally present in the solution phase at around pH 2.6. The proposed reactions for the deprotonation of pyruvic acid by surface hydroxyl groups in ketone and diol forms are shown below respectively:

$$Ti\text{-}OH + CH_3COCOOH \rightarrow CH_3COCOO\text{-}Ti + H_2O \qquad \text{(Eq3.4)}$$

$$Ti\text{-}OH + CH_3C(OH)_2COOH \rightarrow CH_3C(OH)_2COO\text{-}Ti + H_2O \qquad \text{(Eq3.5)}$$

As pH increases to pH 5 and 8, the observed adsorption mechanism on $TiO_2$ is similar to pyruvic acid adsorption at pH 2.6. Figure 3.10 compares the solution phase spectra and adsorption spectra of pyruvic acid at pH 5 and 8. Upon adsorption of pyruvic acid at pH 5, the bands associated with the asymmetric and symmetric stretching vibrations of $COO^-$, at 1635 and 1387 $cm^{-1}$, respectively, increase in intensity. Similarly, there is an increase in peak intensity associated with the asymmetric and symmetric stretching vibrations of $COO^-$ at 1633 and 1385 $cm^{-1}$, respectively, when pyruvic acid at pH 8 adsorbs on $TiO_2$. Therefore, for pyruvic acid solutions between pH 2.6 and 8, further deprotonation occurs on the surface, and pyruvate is formed. As discussed earlier, the fraction of diol species in solution pH 5 and 8 is extremely low in comparison to the fraction of ketone species, so it is expected to observe more ketone species adsorbed on the surface at pH 5 and 8. However, the ketone specie is not observed on the adsorption spectra at pH 5 and 8 because the peak associated with C=O in ketone group at 1709 $cm^{-1}$ is not present. In addition, the adsorption spectra at pH 5 and 8 both, respectively, have peaks at 1140 and 1142 $cm^{-1}$, which is associated with the C-O stretching vibration in alcohols, and thus suggests the presence of diol species on the surface. The unexpected prominent presence of diol species on the surface in more basic solutions suggests that the adsorption of pyruvic acid on $TiO_2$ induces a change in equilibrium for ketone and diol species.

### 3.2.2 Adsorption Reversibility and Binding Mode

In order to address the reversibility adsorption of pyruvic acid on $TiO_2$, the surface was flushed with Milli-Q water at the given pH of the pyruvic acid solution. Figure 3.11 shows the spectra collected after desorption for the three pH values. Although there is a decrease in peak intensities, pyruvate still remains on the surface after desorption for all three pH values, which indicates that pyruvic acid and its different forms irreversibly adsorbs on the surface.

The frequency differences of asymmetric and symmetric stretching vibrations of $COO^-$ for pyruvate on $TiO_2$ surface at pH 2.6, 5, and 8 are 264, 248, and 248 $cm^{-1}$, respectively. Since the frequency difference is roughly between 150 and 260 $cm^{-1}$, the type of binding occurring between pyruvate and $TiO_2$ surface at the three pH values is bidentate bridging. Schematics of the proposed binding mode for pyruvic acid, in ketone and diol form, on $TiO_2$ is illustrated in Figure 3.12.

### 3.2.3 Adsorption Intensity as *f*(pH)

Figure 3.13 shows the adsorption of pyruvic acid on $TiO_2$ nanoparticles with varying solution pH between 3.0 and 7.5. In order to qualitatively observe the amount of adsorption occurring on the surface as a function of pH, the peak intensity associated to the symmetric stretching vibration of $COO^-$ at 1385 $cm^{-1}$, which is representative of pyruvate species, will be examined. Similar to lactic acid, the general trend of pyruvic acid adsorption on $TiO_2$ nanoparticles is that it decreases as solution pH increases due to the increasing repulsive electrostatic interactions between the negatively-charged $TiO_2$ nanoparticles and anions from pyruvate molecules in solution.

## 3.3 Conclusions

The interactions of lactic acid and pyruvic acid on $TiO_2$ are found to exhibit some similarities yet some differences. Upon adsorption, both lactic acid and pyruvic acid are deprotonated by the surface hydroxyl groups and form lactate and pyruvate, respectively. The two oxygen atoms from the carboxylate group bind to two $Ti^{4+}$ ions on the surface via bidentate bridging, and this strong electrostatic interaction results in an irreversible adsorption for lactic acid and pyruvic acid. As solution pH increases, the adsorption intensity decreases for both

carboxylic acids due to the increasing repulsion between the carboxylate anions in solution and negatively-charged $TiO_2$ nanoparticles. The main difference between lactic acid and pyruvic acid is that surface speciation and bulk solution speciation remain constant for lactic acid as a function of pH, but surface speciation differs from bulk solution speciation for pyruvic acid at higher pH values due to the increased presence of diol species adsorbed on $TiO_2$. An overarching molecular picture of lactic acid and pyruvic acid binding on $TiO_2$ surface in the aqueous phase as a function of pH is illustrated in Figures 3.14 and 3.15, respectively.

## 3.4 Acknowledgements

The author of this thesis would like to thank all co-authors and Man Luo for the NMR data used in this chapter. This study was funded by Alfred P. Sloan Foundation under grant number 9-2017-9692.

Chapter 3, in full, is currently being prepared for submission for publication of the material: Tam, R. L.; Shrestha, M.; Grassian, V. H. Surface Chemistry and Adsorption Kinetics for Indoor Relevant Carboxylic Acids in Aqueous Solutions onto $TiO_2$ Nanoparticles: A Study of pH. The thesis author is the primary investigator and author of this paper.

## 3.5 Figures

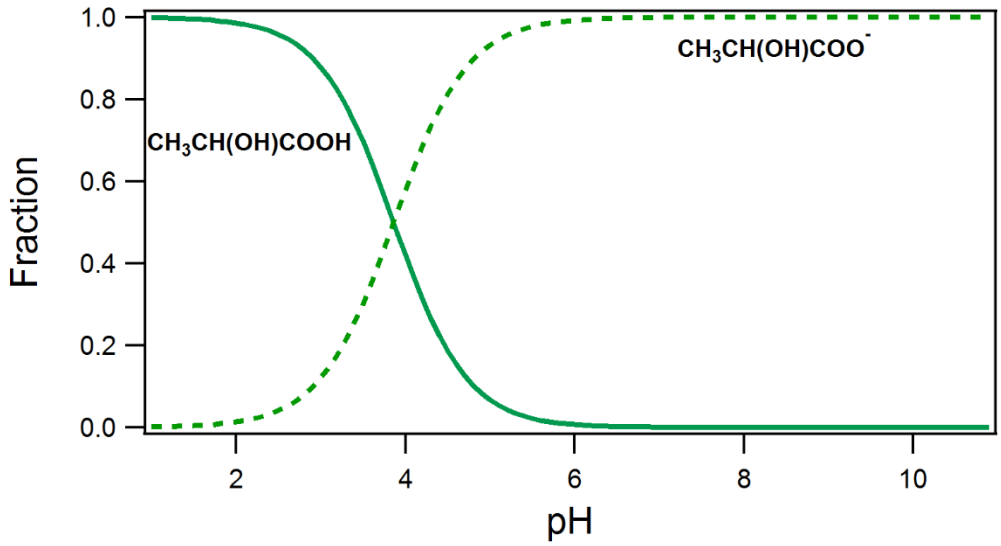


**Figure 3.1:** Speciation diagram of lactic acid, with pKa value of 3.86, in pH range 1 – 11. Fraction of lactic acid and lactate species were calculated with equations 3.1 and 3.2.

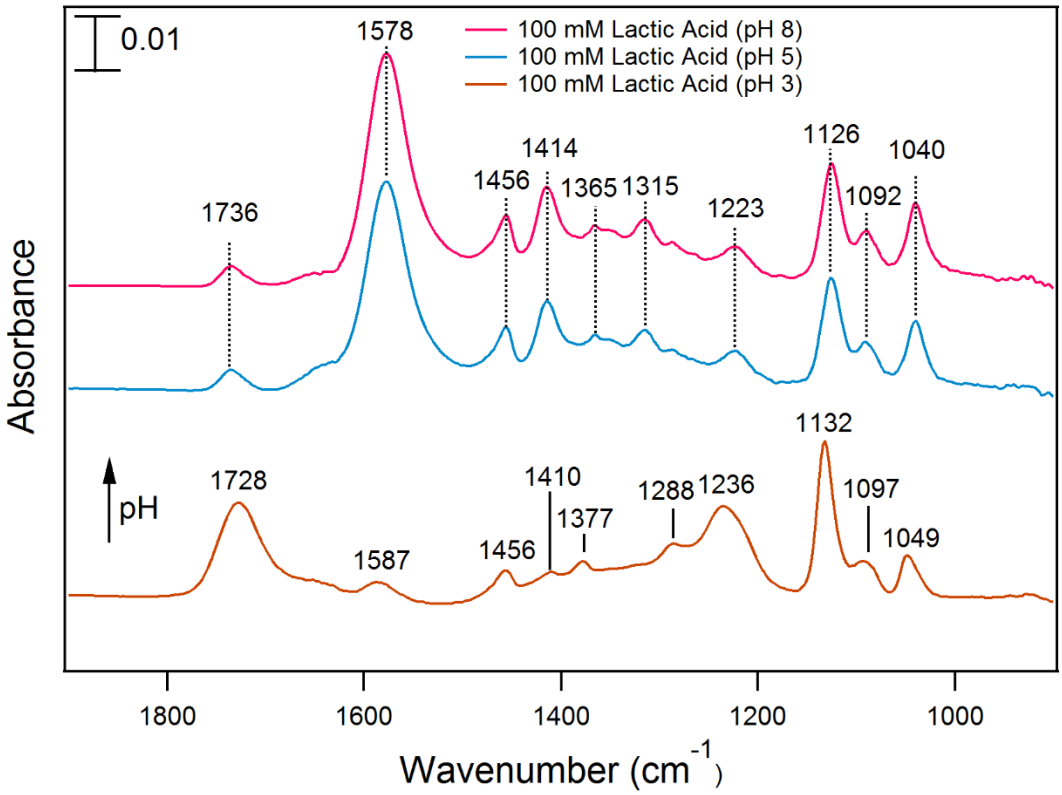


**Figure 3.2:** ATR-FTIR spectra of 100 mM lactic acid in solution phase at three different pH values: pH 3 (–), pH 5 (–), and pH 8 (–). High concentration used for solution phase spectra in order to clearly see the peaks associated to lactic acid.

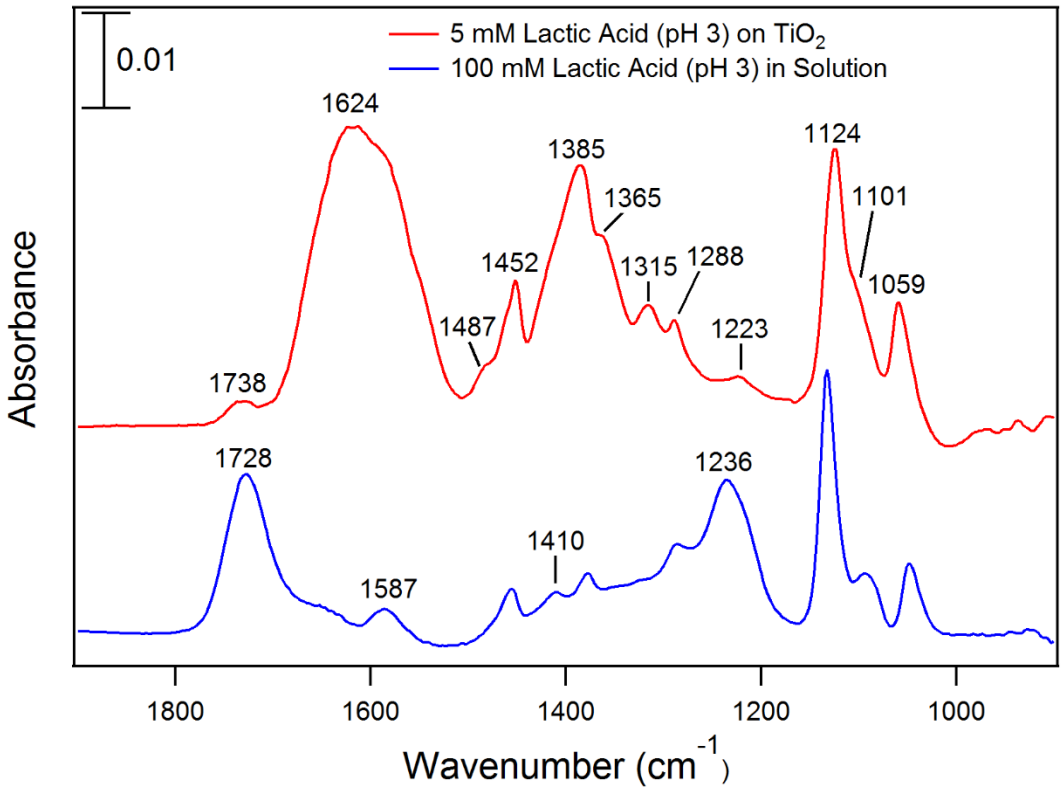


**Figure 3.3:** ATR-FTIR spectra of 100 mM lactic acid at pH 3 in solution phase (–) and 5 mM lactic acid at pH 3 adsorbed onto $TiO_2$ (–).

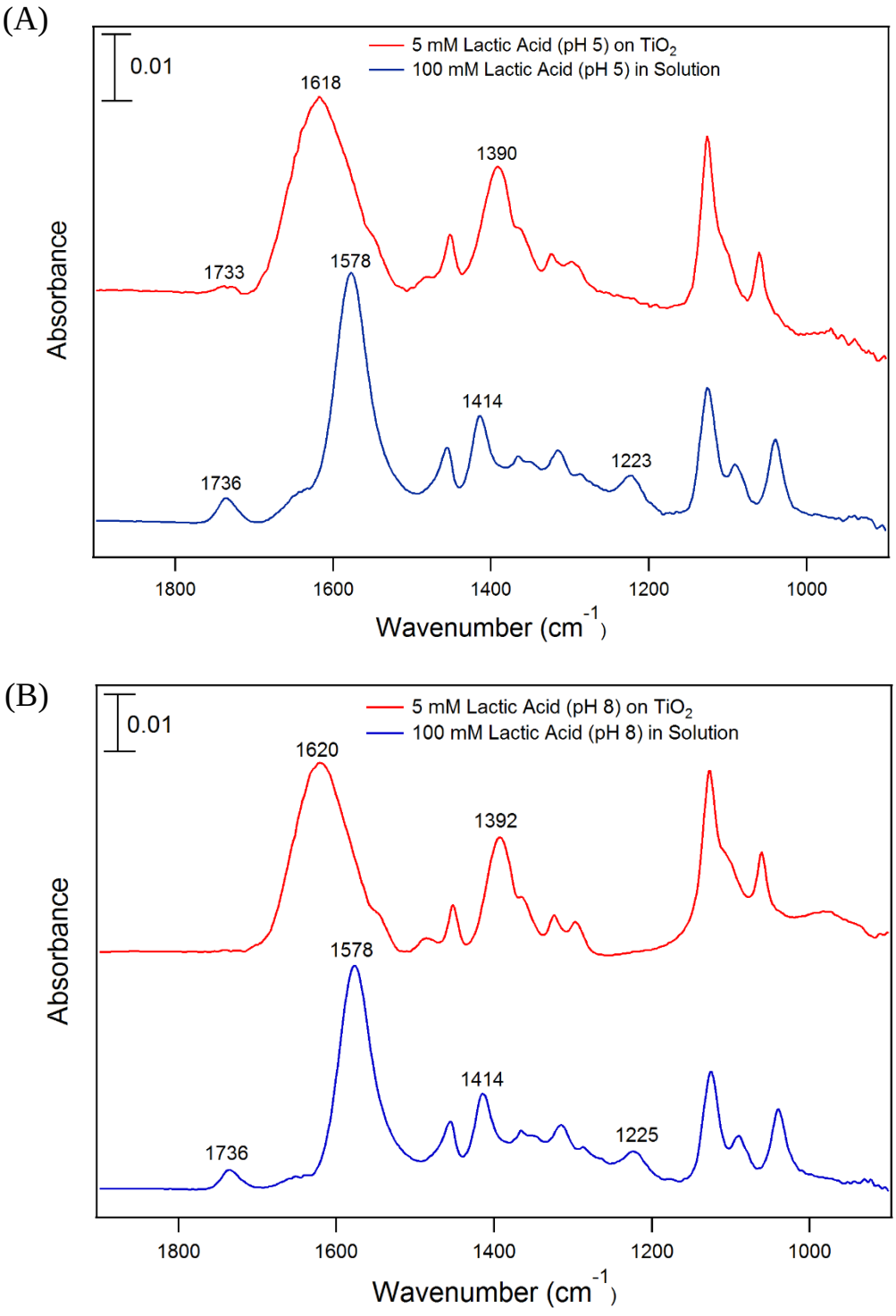


**Figure 3.4:** ATR-FTIR spectra of 100 mM lactic acid in solution phase (–) and 5 mM lactic acid adsorbed onto $TiO_2$ (–), which were both adjusted to two indoor-relevant pHs: (A) pH 5 (B) pH 8. Peaks on the adsorption spectra that are discussed in the chapter are assigned in this figure. Remaining peaks on the adsorption spectra for pH 5 and 8 have similar peak assignments to the adsorption spectrum of lactic acid at pH 3, which can be found on Table 3.2(b).

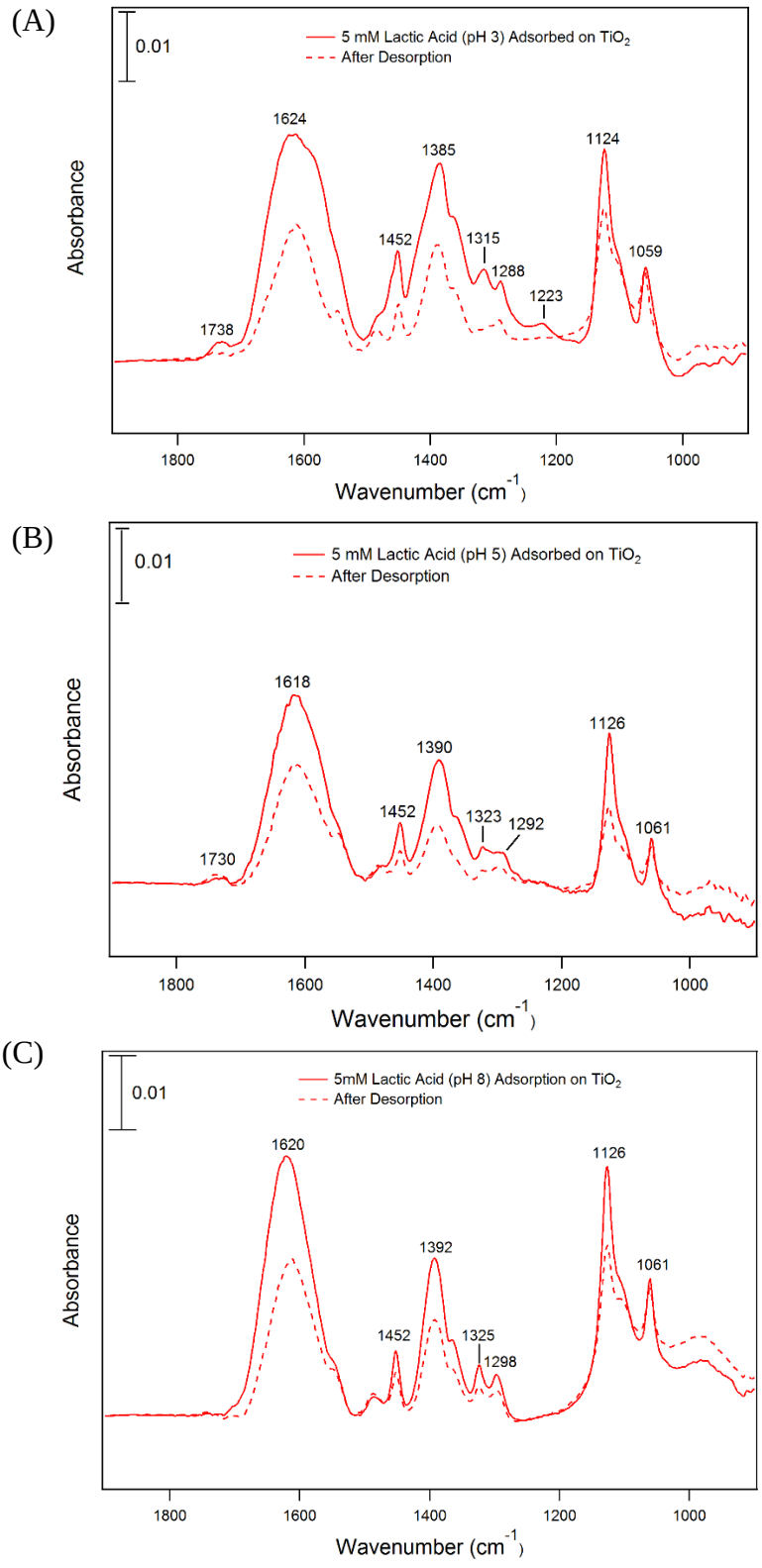


**Figure 3.5:** Adsorption and desorption ATR-FTIR spectra of 5 mM lactic acid on $TiO_2$ at three different pH values: (A) pH 3 (B) pH 5 (C) pH 8.

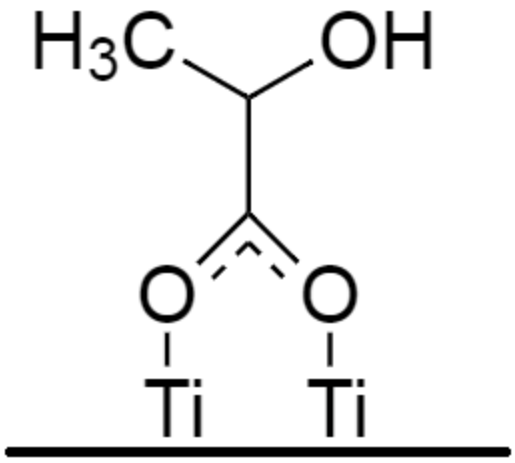


**Figure 3.6:** Schematic of lactic acid adsorbed on $TiO_2$ nanoparticle surface via bidentate bridging. This binding coordination was determined by the frequency difference of asymmetric and symmetric stretching vibrations of $COO^-$.

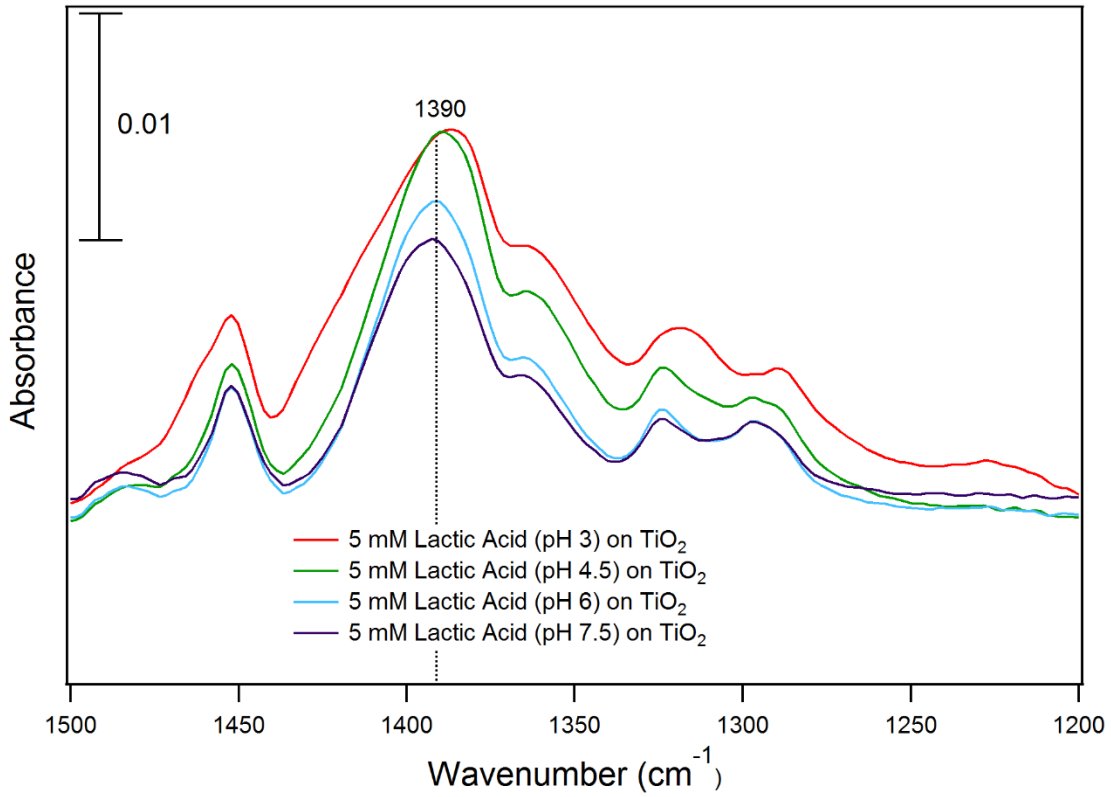


**Figure 3.7:** ATR-FTIR spectra of 5 mM lactic acid adsorbed on $TiO_2$ at different solution pH between 3 and 7.5. Peak at around 1390 $cm^{-1}$ on adsorption spectra is assigned to the symmetric stretching vibration of $COO^-$, which is representative of lactate. Peak intensity decreases as pH increases due to increased repulsion between the lactate anions in solution and negatively-charged $TiO_2$ nanoparticles.

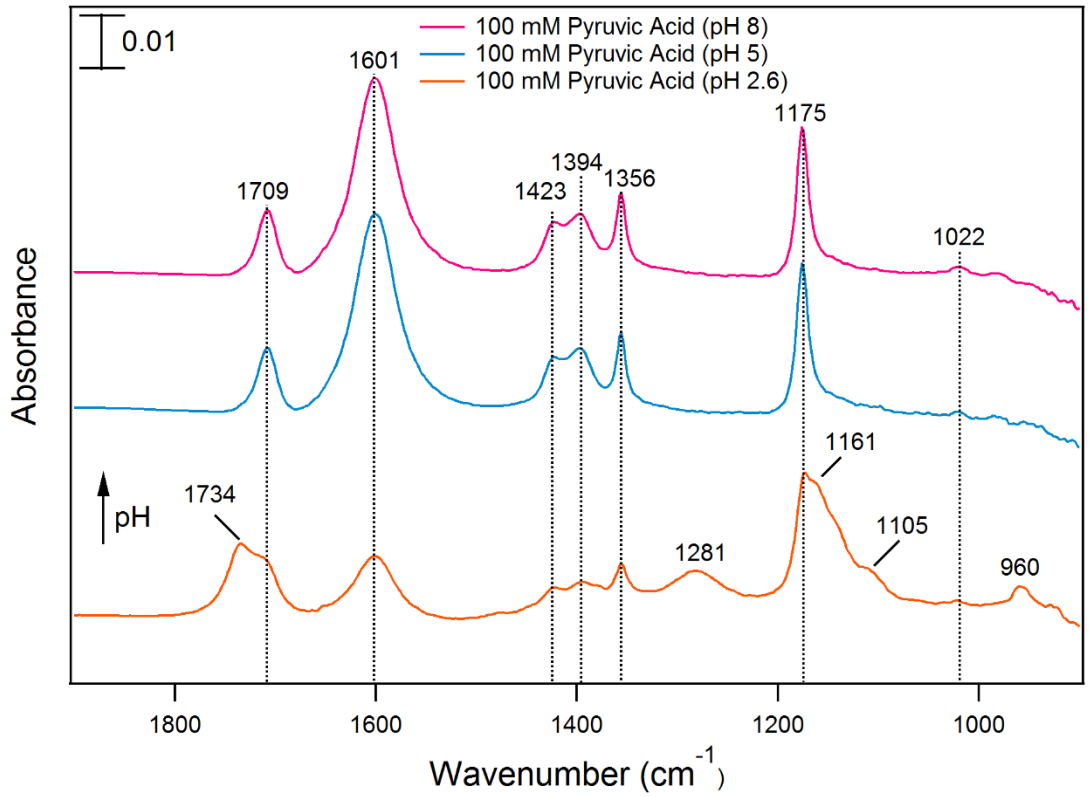


**Figure 3.8:** ATR-FTIR spectra of 100 mM pyruvic acid in solution phase at three different pH values: pH 2.6 (–), pH 5 (–), and pH 8 (–). High concentration used for solution phase spectra in order to clearly see the peaks associated to pyruvic acid.

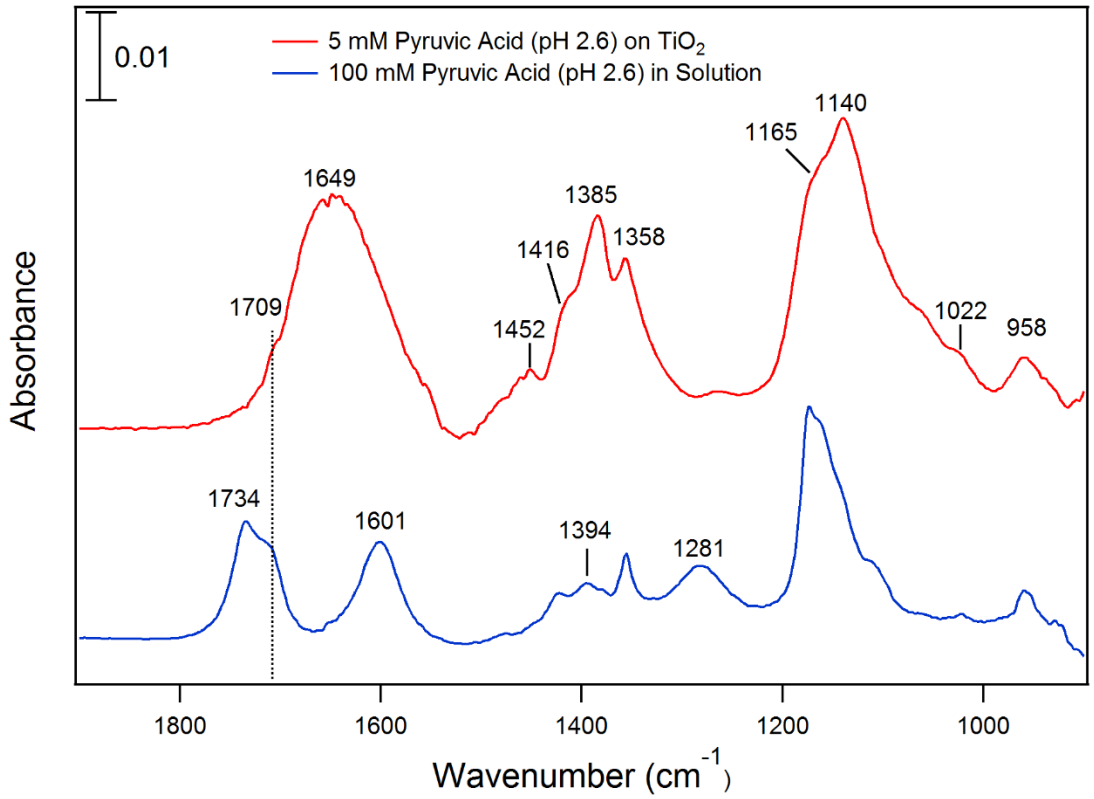


**Figure 3.9:** ATR-FTIR spectra of 100 mM pyruvic acid at pH 2.6 in solution phase (–) and 5 mM pyruvic acid at pH 2.6 adsorbed onto $TiO_2$ (–).

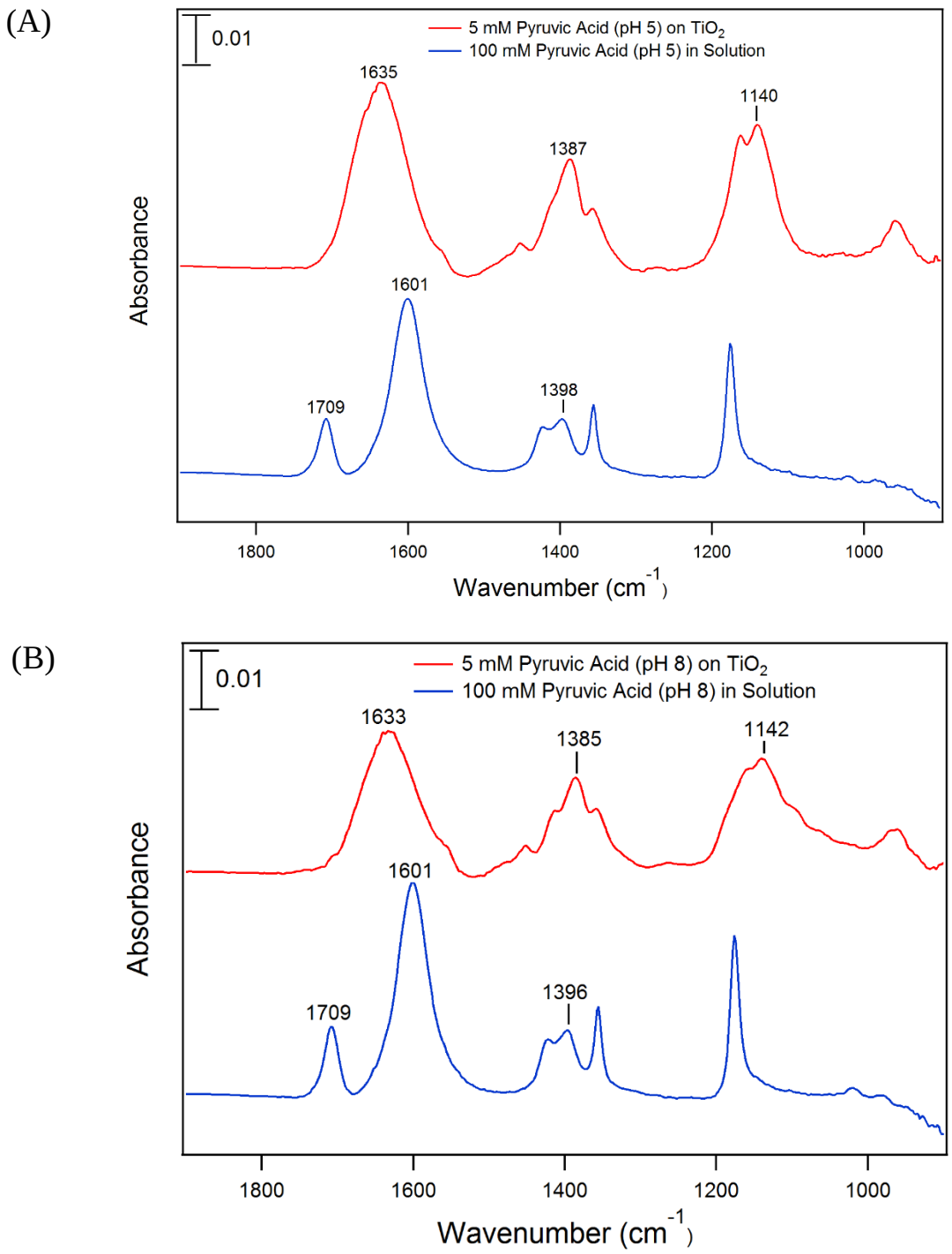


**Figure 3.10:** ATR-FTIR spectra of 100 mM pyruvic acid in solution phase (–) and 5 mM pyruvic acid adsorbed onto $TiO_2$ (–), which were both adjusted to two indoor-relevant pHs: (A) pH 5 (B) pH 8. Peaks on the adsorption spectra that are discussed in the chapter are assigned in this figure. Remaining peaks on the adsorption spectra for pH 5 and 8 have similar peak assignments to the adsorption spectrum of pyruvic acid at pH 2.6, which can be found on Table 3.5(b).

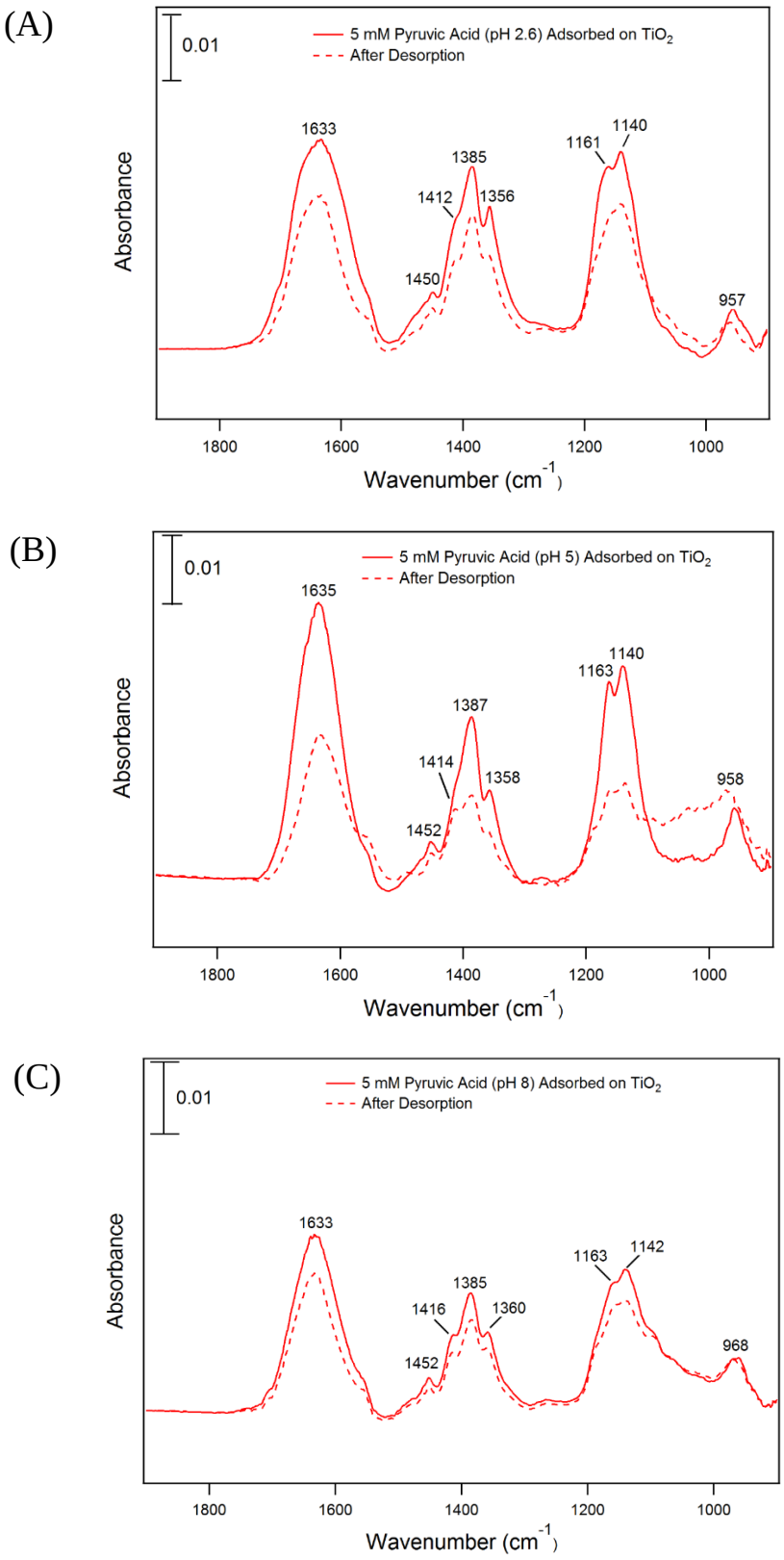


**Figure 3.11:** Adsorption and desorption ATR-FTIR spectra of 5 mM pyruvic acid on $TiO_2$ at three different pH values: (A) pH 2.6 (B) pH 5 (C) pH 8.

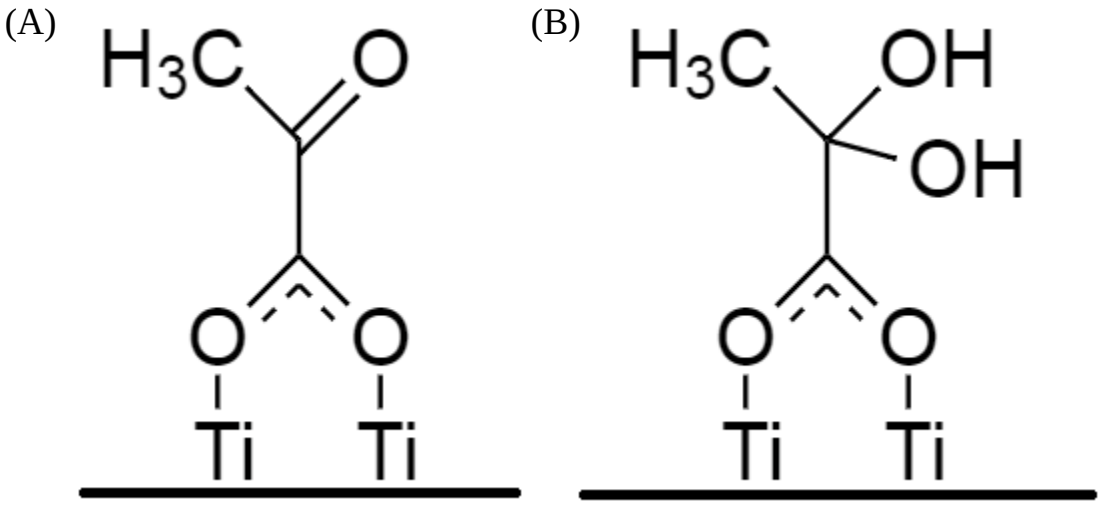


**Figure 3.12:** Schematics of pyruvic acid adsorbed on $TiO_2$ nanoparticle surface via bidentate bridging (A) Ketone species (B) Diol species. This binding coordination was determined by the frequency difference of asymmetric and symmetric stretching vibrations of $COO^-$.

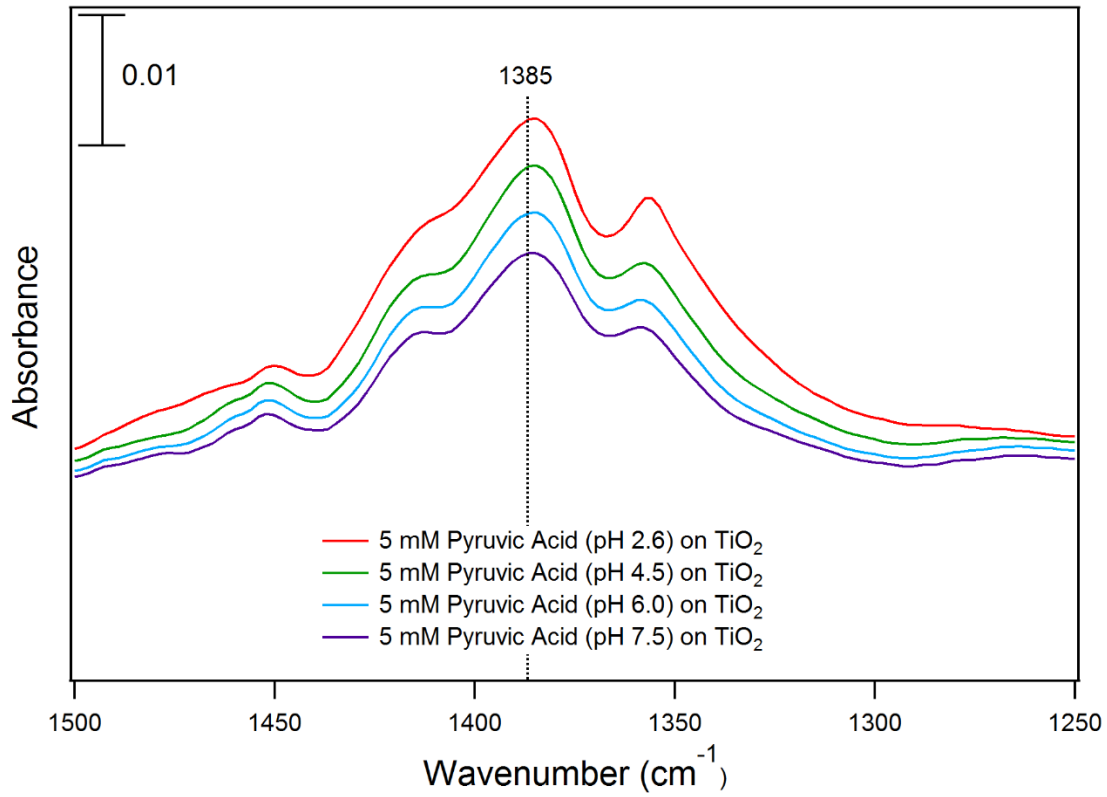


**Figure 3.13:** ATR-FTIR spectra of 5 mM pyruvic acid adsorbed on $TiO_2$ at different solution pH between 3 and 7.5. Peak at 1385 $cm^{-1}$ on adsorption spectra is assigned to the symmetric stretching vibration of $COO^-$, which is representative of pyruvate. Peak intensity decreases as pH increases due to increased repulsion between the pyruvate anions in solution and negatively-charged $TiO_2$ nanoparticles.

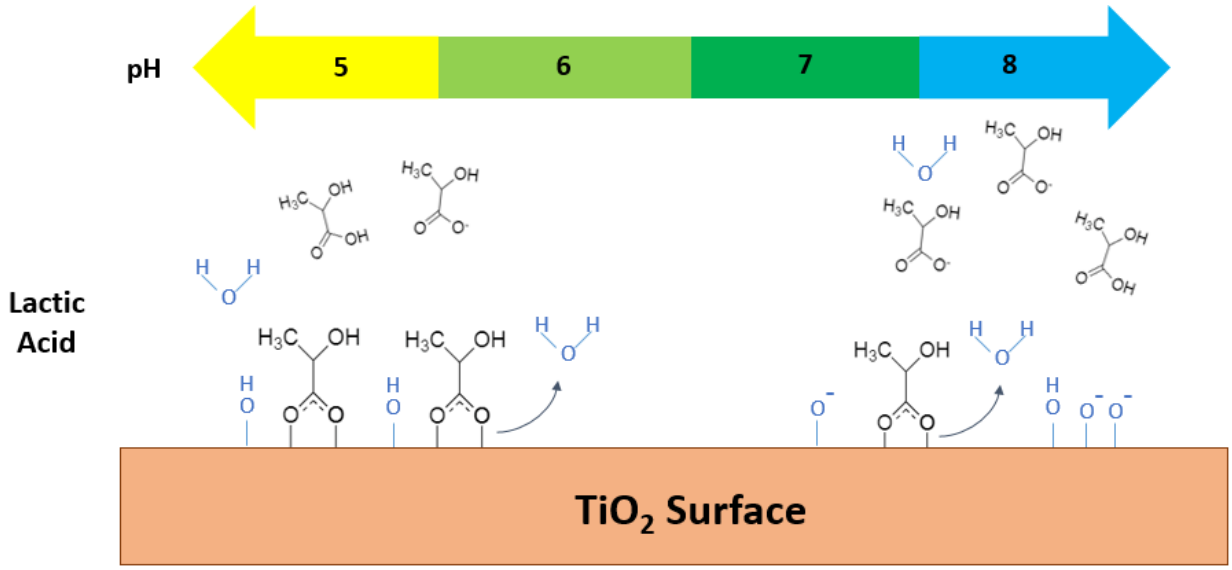


**Figure 3.14:** An overarching molecular picture of lactic acid partitioned into a thin water film that is on a $TiO_2$ surface and binding on the $TiO_2$ surface as a function of indoor-relevant pH values.

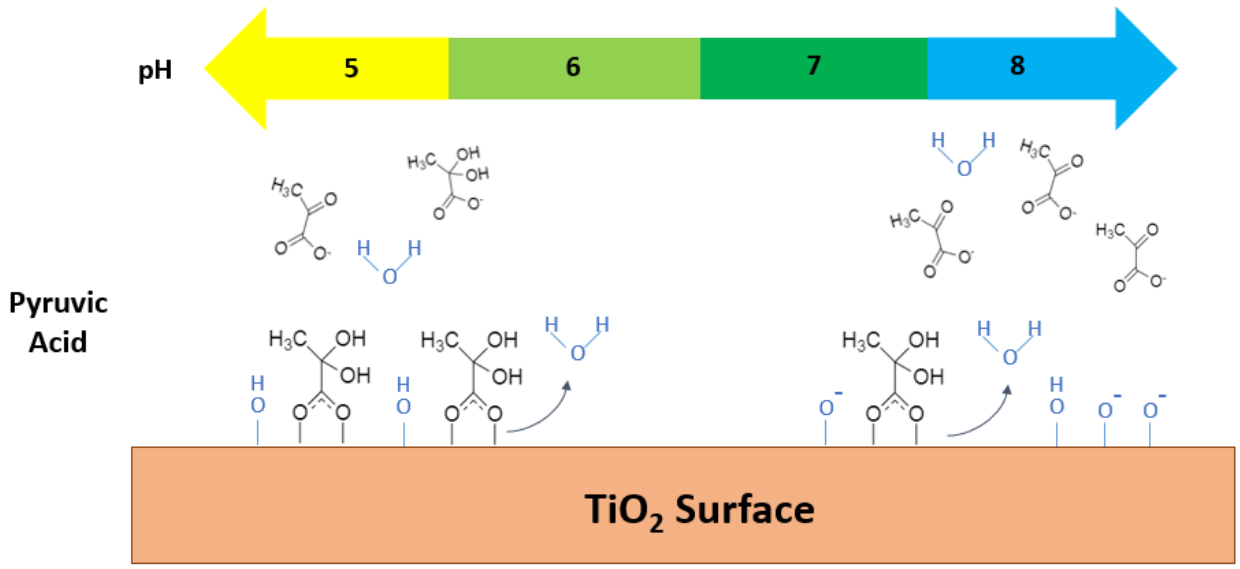


**Figure 3.15:** An overarching molecular picture of pyruvic acid partitioned into a thin water film that is on a $TiO_2$ surface and binding on the $TiO_2$ surface as a function of indoor-relevant pH values.

## 3.6 Tables

**Table 3.1:** Structure and pKa value for lactic acid ($CH_3CH(OH)COOH$) at 298 K. Red spheres for oxygen atoms, gray spheres for carbon atoms, and white spheres for hydrogen atoms.

| 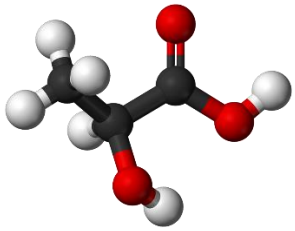 | **pKa** |
|---|---|
| **$CH_3CH(OH)COOH \rightleftharpoons H^+ + CH_3CH(OH)COO^-$** | 3.86 |

**Table 3.2(a):** Band assignments and frequencies ($cm^{-1}$) of 100 mM lactic acid (pH 3) in aqueous solution. Literature values come from Cassanas, G.; Morssli, M.; Fabregue, E.; Bardet, L. Vibrational Spectra of Lactic Acid and Lactates. *Journal of Raman Spectroscopy*. **1991**, *22*, 409-413.

| Solution-Phase Mode Assignments | Our Study | Literature |
|---|---|---|
| $\nu$(C=O) | 1728 | 1725 |
| $\nu_{as}(COO^-)$ | 1587 | 1585 |
| $\delta_{as}(CH_3)$ | 1456 | 1455 |
| $\nu_s(COO^-)$ | 1410 | 1420 |
| $\delta s(CH_3)$, $\delta$(OH) | 1377 | 1380 |
| $\delta_{AL}$(OH) | 1288 | 1285 |
| $[\delta_{AC}(CO) + \delta_{AC}(OH)]$ | 1236 | 1240 |
| $\rho(CH_3)$, $\nu_{AL}$(CO) | 1132 | 1130 |
| $\nu_{AL}$(CO) | 1097 | 1090 |
| $\nu$(C-$CH_3$) | 1049 | 1050 |

*AL = alcohol; AC = acid

**Table 3.2(b):** Band assignments and frequencies ($cm^{-1}$) of 5 mM lactic acid (pH 3) adsorbed on $TiO_2$ surface. Literature values come from gas-phase adsorption study on lactic acid and $TiO_2$: Chen, Y. K.; Lin, Y. F.; Peng, Z. W.; Lin, J. L. Transmission FT-IR Study on the Adsorption and Reactions of Lactic Acid and Poly(lactic acid) on $TiO_2$. *J. Phys. Chem. C*. **2010**, *114*, 17720-17727.

| $TiO_2$ Adsorption Mode Assignments | Our Study | Literature |
|---|---|---|
| $\nu$(C=O) | 1738 | 1722 |
| $\nu_{as}(COO^-)$ | 1624 | 1569 |
| $\delta_{as}(CH_3)$ | 1487, 1452 | 1470, 1456 |
| $\nu_s(COO^-)$ | 1385 | 1421 |
| $\delta s(CH_3)$, $\delta$(OH) | 1365 | 1376 |
| $\delta$(CH) | 1315 | 1305 |
| $\delta_{AL}$(OH) | 1288 | 1269 |
| $[\delta_{AC}(CO) + \delta_{AC}(OH)]$ | 1223 | 1220 |
| $\rho(CH_3)$, $\nu_{AL}$(CO) | 1124 | 1130 |
| $\nu_{AL}$(CO) | 1101 | 1102 |
| $\nu$(C-$CH_3$) | 1059 | 1052 |

*AL = alcohol; AC = acid

**Table 3.3:** Band assignments and frequencies ($cm^{-1}$) of 100 mM lactic acid (pH 5 and 8) in aqueous solution. Literature values come from Cassanas, G.; Morssli, M.; Fabregue, E.; Bardet, L. Vibrational Spectra of Lactic Acid and Lactates. *Journal of Raman Spectroscopy*. **1991**, *22*, 409-413.

| Solution-Phase Mode Assignments | Our Study | Literature |
|---|---|---|
| $\nu(C=O)$ | 1736 | 1725 |
| $\nu_{as}(COO^-)$ | 1578 | 1585 |
| $\delta_{as}(CH_3)$ | 1456 | 1455 |
| $\nu_s(COO^-)$ | 1414 | 1420 |
| $\delta s(CH_3)$, $\delta(OH)$ | 1365 | 1380 |
| $\delta_{AL}(OH)$ | 1315 | 1285 |
| $[\delta_{AC}(CO) + \delta_{AC}(OH)]$ | 1223 | 1240 |
| $\rho(CH_3)$, $\nu_{AL}(CO)$ | 1126 | 1130 |
| $\nu_{AL}(CO)$ | 1092 | 1090 |
| $\nu(C\text{-}CH_3)$ | 1040 | 1050 |

*AL = alcohol; AC = acid

**Table 3.4:** Structures and percent fraction for four species of pyruvic acid in $H_2O$ at different pH values. Percent fractions were experimentally determined with NMR spectroscopy, and data produced by Grassian group member, Man Luo. Experimental speciation is in good agreement with previous literature: Rapf, R. J.; Dooley, M. R.; Kappes, K.; Perkins, R. J.; Vaida, V. pH Dependence of the Aqueous Photochemistry of α-Keto Acids. *J Phys. Chem. A.* **2017**, *121*, 8368-8379.

| | 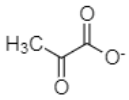 | 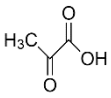 | 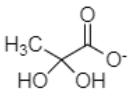 | 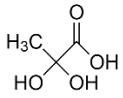 |
|---|---|---|---|---|
| **pH** | **Ketone anion (%)** | **Ketone neutral (%)** | **Diol anion (%)** | **Diol neutral (%)** |
| 1.11 | 2.9 | 28.3 | 0.3 | 68.5 |
| 1.36 | 5.0 | 27.5 | 0.5 | 67.0 |
| 1.54 | 7.4 | 26.8 | 0.7 | 65.2 |
| 1.87 | 14.7 | 25.0 | 1.4 | 58.9 |
| 2.4 | 35.5 | 17.8 | 3.4 | 43.2 |
| 2.92 | 62.7 | 9.5 | 5.8 | 22.0 |
| 3.49 | 80.8 | 3.3 | 7.9 | 8.0 |
| 3.96 | 86.6 | 1.2 | 9.1 | 3.1 |
| 5.12 | 89.0 | 0.1 | 10.6 | 0.3 |
| 7.93 | 89.5 | 0.0 | 10.5 | 0.0 |

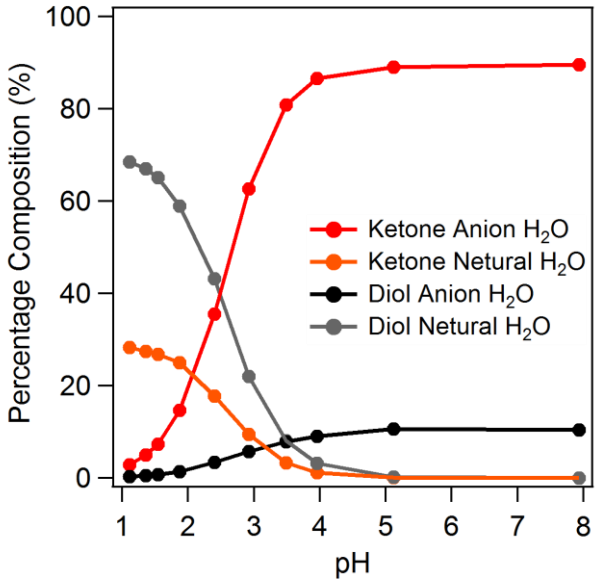

**Table 3.5(a):** Band assignments and frequencies ($cm^{-1}$) of 100 mM pyruvic acid (pH 2.6) in aqueous solution. Literature values from Katon, J. E.; Covington, D. T. The Vibrational Spectra of Crystalline Sodium Pyruvate. *Spectroscopy Letters*. **1979**, *12*, 761-766. And Plath, K. L.; Takahashi, K.; Skodje, R. T.; Vaida, V. Fundamental and Overtone Vibrational Spectra of Gas-Phase Pyruvic Acid. *J. Phys. Chem. A.* **2009**, *113*, 7294-7303.

| Solution Phase Mode Assignments | Our Study | Literature |
|---|---|---|
| $\nu(C=O)_{acid}$ | 1734 | 1791 |
| $\nu(C=O)_{ketone}$ | 1709 | 1709 |
| $\nu_{as}(COO^-)$ | 1601 | 1657 |
| $\delta_{as}(CH_3)$ | 1423 | 1439 |
| $\nu_s(COO^-)$ | 1394 | 1407 |
| $\delta_s(CH_3)$ | 1356 | 1357 |
| $\delta(COH)$ | 1281 | 1245 |
| $\nu(CH_3\text{-}C)$ | 1175 | 1190 |
| $\nu(C\text{-}O)_{alcohol}$ | 1161, 1105 | 1139 |
| $\rho(CH_3)$ | 1022, 960 | 1015, 969 |

**Table 3.5(b):** Band assignments and frequencies ($cm^{-1}$) of 5 mM pyruvic acid (pH 2.6) adsorbed on $TiO_2$. Literature values from gas-phase pyruvic acid adsorption on $TiO_2$: Alves, M. and Fang, Y.; Wall, K.; Grassian, V. H. Surface Chemistry and Photochemistry of Pyruvic Acid on Oxide Surfaces. *In preparation.* And Katon, J. E.; Covington, D. T. The Vibrational Spectra of Crystalline Sodium Pyruvate. *Spectroscopy Letters*. **1979**, *12*, 761-766.

| $TiO_2$ Adsorption Mode Assignments | Our Study | Literature |
|---|---|---|
| $\nu(C=O)_{ketone}$ | 1709 | 1709 |
| $\nu_{as}(COO^-)$ | 1649 | 1610 |
| $\delta(C\text{-}H)$ | 1452 | 1467 |
| $\delta_{as}(CH_3)$ | 1416 | 1411 |
| $\nu_s(COO^-)$ | 1385 | 1407 |
| $\delta_s(CH_3)$ | 1358 | 1359 |
| $\nu(CH_3\text{-}C)$ | 1165 | 1180 |
| $\nu(C\text{-}O)_{alcohol}$ | 1140 | 1139 |
| $\rho(CH_3)$ | 1022, 958 | 1023, 980 |

**Table 3.6:** Band assignments and frequencies ($cm^{-1}$) of 100 mM pyruvic acid (pH 5 and 8) in aqueous solution. Literature values from Katon, J. E.; Covington, D. T. The Vibrational Spectra of Crystalline Sodium Pyruvate. *Spectroscopy Letters*. **1979**, *12*, 761-766. And Plath, K. L.; Takahashi, K.; Skodje, R. T.; Vaida, V. Fundamental and Overtone Vibrational Spectra of Gas-Phase Pyruvic Acid. *J. Phys. Chem. A*. **2009**, *113*, 7294-7303.

| **Solution Phase Mode Assignments** | **Our Study** | **Literature** |
|---|---|---|
| $\nu(C=O)_{ketone}$ | 1709 | 1709 |
| $\nu_{as}(COO^-)$ | 1601 | 1657 |
| $\delta_{as}(CH_3)$ | 1423 | 1439 |
| $\nu_s(COO^-)$ | 1394 | 1407 |
| $\delta_s(CH_3)$ | 1356 | 1357 |
| $\nu(CH_3\text{-}C)$ | 1175 | 1190 |
| $\rho(CH_3)$ | 1022 | 1015 |

## 3.7 References


1. Liu, S.; Thompson, S. L.; Stark, H.; Ziemann, P. J.; Jimenez, J. L. Gas-Phase Carboxylic Acids in a University Classroom: Abundance, Variability, and Sources. *Environ. Sci. Technol*. **2017**, *51*, 5454-5463.

2. Duncan, S. M.; Sexton, K. G.; Turpin, B. J. Oxygenated VOCs, aqueous chemistry, and potential impacts on residential indoor air composition. *Indoor Air*. **2018**, *28*, 198-212.

3. Ube, T.; Yoneyama, Y.; Ishiguro, T. *In situ* Measurement of the pH-dependent Transmission Infrared Spectra of Aqueous Lactic Acid Solutions. *Analytical Sciences*. **2017**, *33*, 1395-1400.

4. Chen, Y. K.; Lin, Y. F.; Peng, Z. W.; Lin, J. L. Transmission FT-IR Study on the Adsorption and Reactions of Lactic Acid and Poly(lactic acid) on $TiO_2$. *J. Phys. Chem. C*. **2010**, *114*, 17720-17727.

5. Mudunkotuwa, I. A.; Grassian, V. H. Citric Acid Adsorption on $TiO_2$ Nanoparticles in Aqueous Suspensions at Acidic and Circumneutral pH: Surface Coverage, Surface Speciation, and Its Impact on Nanoparticle-Nanoparticle Interactions. *J. Am. Chem. Soc*. **2010**, *132*, 14986-14994.

6. Jayalath, S.; Wu, H.; Larsen, S. C.; Grassian, V. H. Surface Adsorption of Suwannee River Humic Acid on $TiO_2$ Nanoparticles: A Study of pH and Particle Size. *Langmuir*. **2018**, *34*, 3136-3145.

7. Dobson, K. D.; McQuillan, A. J. In situ Infrared Spectroscopic Analysis of the Adsorption of Aromatic Carboxylic Acids to $TiO_2$, $ZrO_2$, $Al_2O_3$, and $Ta_2O_5$ From Aqueous Solutions. *Spectrochim. Acta, Part A*. **2000**, *56*, 557-565.

8. Nara, M.; Torii, H.; Tasumi, M. Correlation between the Vibrational Frequencies of the Carboxylate Group and the Types of Its Coordination to a Metal Ion: An ab Initio Molecular Orbital Study. *J. Phys. Chem*. **1996**, *100*, 19812-19817.

9. Rapf, R. J.; Dooley, M. R.; Kappes, K.; Perkins, R. J.; Vaida, V. pH Dependence of the Aqueous Photochemistry of α-Keto Acids. *J Phys. Chem. A*. **2017**, *121*, 8368-8379.

10. Alves, M. and Fang, Y.; Wall, K.; Grassian, V. H. Surface Chemistry and Photochemistry of Pyruvic Acid on Oxide Surfaces. *In preparation.*

# Chapter 4 Adsorption Kinetics and Quantitative Surface Coverage of Lactic Acid and Pyruvic Acid on $TiO_2$ Nanoparticles: A Study of pH Effects

## 4.1 Adsorption Kinetics Determined via ATR-FTIR

In addition to studying surface adsorption as function of pH, ATR-FTIR spectroscopy was also used to investigate the adsorption and desorption kinetics of lactic acid and pyruvic acid on $TiO_2$ nanoparticles at different pH values. Kinetics for solutions at pH 5 and 8 were specifically studied as these have the most relevance to indoor environments. Adsorption and desorption spectra were collected every five minutes. Integrated peak areas between 1506 and 1269 $cm^{-1}$ for lactic acid and 1525 and 1284 $cm^{-1}$ for pyruvic acid, which are highlighted in the yellow box shown in Figures 4.1 and 4.3, respectively, were used to create the kinetic curves. These spectral regions were selected because they are associated with the absorption associated to the symmetric stretching frequency of lactate and pyruvate, which are at 1390 and 1387 $cm^{-1}$, respectively. This absorption was preferred over the peak associated to the asymmetric stretching of lactate and pyruvate, which are at 1618 and 1635 $cm^{-1}$, respectively, because it will not have any contribution from the water absorption band that is usually around 1637 $cm^{-1}$.

### 4.1.1 Lactic Acid

Figure 4.2 shows the adsorption and desorption kinetic curves of 5 mM lactic acid on $TiO_2$ nanoparticles at solution pH 5 and 8. The rate of adsorption is dependent on the concentration of lactic acid in solution and the amount of available surface sites.[1] However, the concentration of lactic acid in solution does not change over time, so it is assumed to be a

constant, which results in the rate of adsorption to be only dependent on the number of available surface sites and thus a pseudo first order reaction.[1] By assuming that the reaction is pseudo first order, an exponential decay model was fit to the initial portion of the kinetic curves in order to determine the experimental rate constants (k). The increasing form of exponential decay model (Eq4.1) was used for adsorption process, and the decreasing form of exponential decay model (Eq4.2) was used for desorption process, where C is the upper boundary limit.

$$f(t) = C\,(1 - e^{-kt}) \qquad \text{(Eq4.1)}$$

$$f(t) = C\,e^{-kt} \qquad \text{(Eq4.2)}$$

The increasing form of exponential decay model was fitted to about the first 10 minutes of adsorption process, and the decreasing form of exponential decay model was fitted to about the first 22 minutes of desorption process. The adsorption and desorption rate constants for solutions at pH 5 and 8 are listed in Table 4.1. The general observed trend is that as solution pH increases, the adsorption and desorption rate constants do not significantly differ from one another.

### 4.1.2 Pyruvic Acid

Figure 4.4 shows the adsorption and desorption kinetic curves of 5 mM pyruvic acid on $TiO_2$ nanoparticles at solution pH 5 and 8. Similar to lactic acid on $TiO_2$, the adsorption of pyruvic acid on $TiO_2$ is pseudo first order, so the exponential decay models (Eq 4.1 and 4.2) are used to determine rate constants for adsorption and desorption process, respectively. The increasing form of exponential decay model was fitted to about the first 10 minutes of adsorption process, and the decreasing form of exponential decay model was fitted to about the first 22 minutes of desorption process. Table 4.2 lists the adsorption and desorption rate constants for

pyruvic acid solution at pH values 5 and 8. The overall trend is that adsorption and desorption rate constants do not significantly differ as solution pH increases, which is in good agreement with the observations for lactic acid rate constants.

## 4.2 Surface Coverage of Lactic Acid and Pyruvic Acid Determined via QCM-D

QCM-D, an analytical technique used to measure the amount of mass of adsorbed molecules on a surface, is used in combination with ATR-FTIR spectroscopy to study the adsorption of lactic acid and pyruvic acid on $TiO_2$ surfaces. The benefits for coupling these two analytical techniques is that QCM-D can provide qualitative comparisons to the observations from ATR-FTIR and quantitative data to complement those qualitative trends. For QCM-D experiments, 20 mM lactic acid and pyruvic acid solutions flows across custom-made $TiO_2$ coated quartz crystal sensors. This higher concentration of lactic acid and pyruvic acid was determined to be optimal for our QCM-D experiments because maximum surface coverage is achieved within a reasonable time frame. Although solution concentration and $TiO_2$ surface used in QCM-D is different from ATR-FTIR studies, these measurements are expected to provide additional insights on the interactions of lactic acid and pyruvic acid on $TiO_2$ surface, which will complement the ATR-FTIR data.

Figures 4.5 and 4.6 show the normalized change in frequency and dissipation over time during the adsorption-desorption process of lactic acid and pyruvic acid, respectively, and similar to the ATR-FTIR kinetics studies, only solutions with indoor-relevant pH values of 5 and 8 were investigated in these QCM-D studies. As the adsorbates are introduced onto the $TiO_2$ coated crystal, the frequency begins to decrease while the dissipation begins to increase. The decrease

in frequency correlates to an increase of molecules adsorbing on the surface, and the increase in dissipation relates to how much the adsorbed layer deforms when the crystal oscillates. As explained in Chapter 2, an adsorbed film is considered rigid when there is little discrepancy in dissipation between different overtones; therefore, it is suggested that lactic acid and pyruvic acid are rigidly adsorbed on $TiO_2$ in both pH 5 and 8 solution environments. In addition, since the change in dissipation does not exceed 2 ppm, the adsorbed film is considered thin and rigid enough that the Sauerbrey equation (Eq2.3) can be applied to determine the mass of adsorbed molecules per surface area from the change in frequency.[2] Figure 4.7 illustrates the change in mass over time, which was determined by the Sauerbrey equation, during the adsorption-desorption process of lactic acid and pyruvic acid solution at pH 5 and 8. The calculated number of adsorbed molecules per surface area after the adsorption and desorption steps are listed in Table 4.3. For both carboxylic acids, more carboxylate molecules are adsorbed on the surface from solution at pH 5 than pH 8. Specifically, the number of lactate molecules adsorbed on $TiO_2$ at pH 5 and 8 after the adsorption step are, respectively, 14.3 and 6.22 x $10^{14}$ molecules/$cm^2$, and the number of pyruvate molecules adsorbed on $TiO_2$ at pH 5 and 8 after the adsorption step are, respectively, 21.9 and 15.8 x $10^{14}$ molecules/$cm^2$. These mass calculations support the qualitative observations from ATR-FTIR and confirms that less adsorption occurs as solution pH increases.

To determine whether the adsorption of lactic acid and pyruvic acid is irreversible, Milli-Q $H_2O$ is re-introduced after adsorption. There is a small increase in frequency at the beginning, but equilibrium is achieved very quickly as frequency remains constant for the remainder of desorption period. This observation suggests that majority of lactate and pyruvate remains on the surface after desorption, which is in good agreement with the qualitative ATR-FTIR

observations in Chapter 3. In addition, there is a decrease in dissipation upon desorption, and this change signifies that loosely bounded molecules were removed when the surface was washed and the remaining adsorbed compounds on the surface are rigidly attached. These measurements well support the ATR-FTIR observations that adsorption of lactic acid and pyruvic acid on $TiO_2$ is irreversible due to strong bidentate binding.

## 4.3 Conclusion

The reaction order for lactic acid and pyruvic acid are both pseudo first order, and the kinetic trends of lactic acid and pyruvic acid on $TiO_2$ at different solution pH are similar to one another. Adsorption rate constants decrease as pH increases, while desorption rate constants increase as pH increases. This trend in rate constants supports the following suggestions: as solution pH increases, the decreasing number of available positively-charged surface sites slows down adsorption rate, and the increasing repulsion between anions in solution and negatively-charged $TiO_2$ nanoparticles weakens attractive electrostatic interactions and thus increases desorption rate. In addition, the decreasing adsorption rate constant as pH increases quantitatively supports the observations of lower adsorption intensity for higher pH values.

QCM-D data also confirms the qualitative ATR-FTIR observations that suggest adsorption of lactic acid and pyruvic acid on $TiO_2$ surface decreases as pH increases. Number of adsorbed molecules on the surface was calculated with the Sauerbrey equation, and the amount of lactate and pyruvate molecules on $TiO_2$ is greater for solutions at pH 5 than pH 8. Additionally, the irreversibility of lactic acid and pyruvic acid adsorption on $TiO_2$ observed in ATR-FTIR studies was confirmed with QCM-D as well.

## 4.4 Acknowledgements

The author of this thesis would like to thank all co-authors. This study was funded by Alfred P. Sloan Foundation under grant number 9-2017-9692.

Chapter 4, in full, is currently being prepared for submission for publication of the material. Tam, R. L.; Shrestha, M.; Grassian, V. H. Surface Chemistry and Adsorption Kinetics for Indoor Relevant Carboxylic Acids in Aqueous Solutions onto $TiO_2$ Nanoparticles: A Study of pH. The thesis author is the primary investigator and author of this paper.

## 4.5 Figures

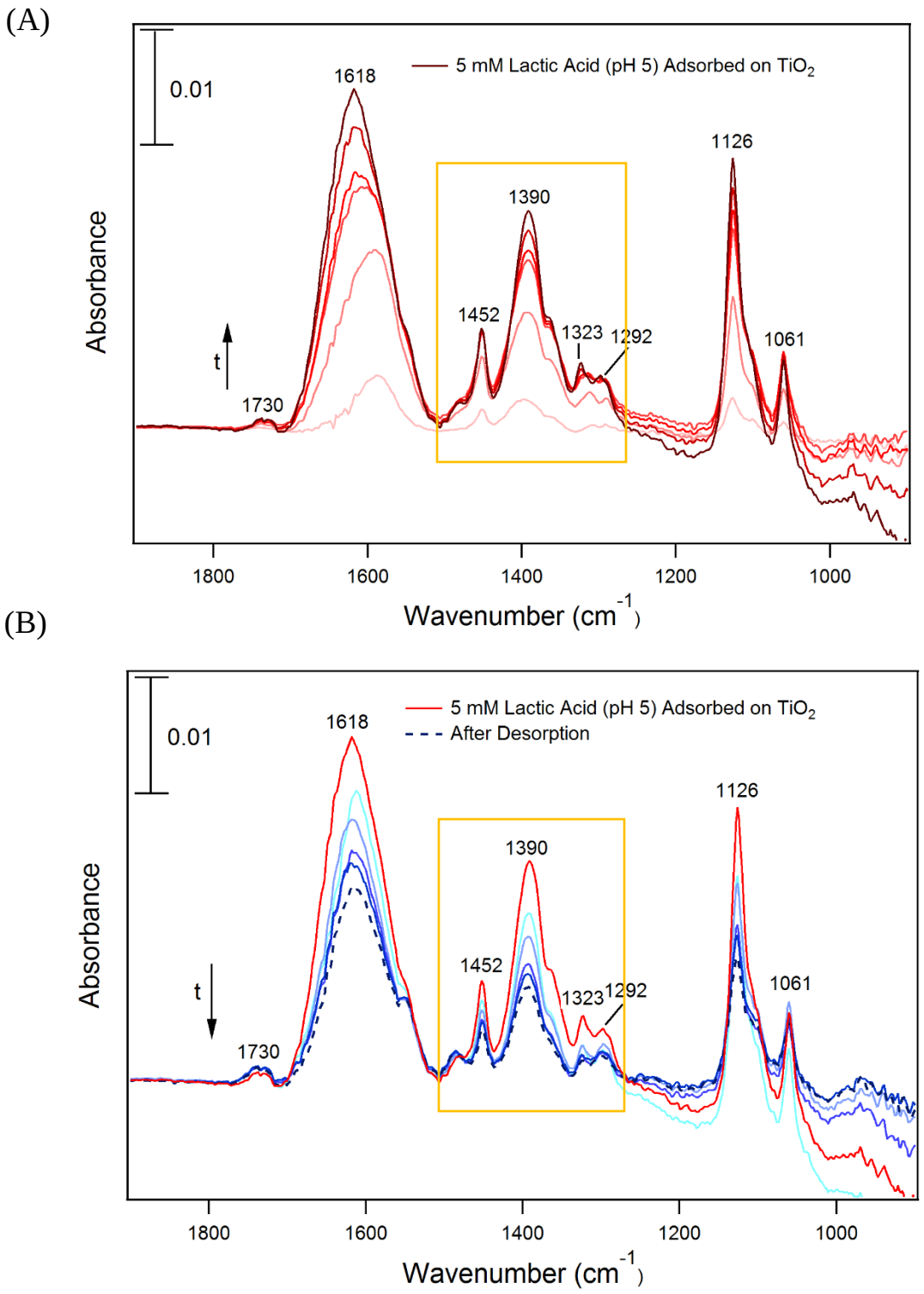


**Figure 4.1:** ATR-FTIR spectra collected every five minutes of 5 mM Lactic Acid (pH 5) on $TiO_2$ nanoparticle surface (A) adsorption process (B) desorption process.

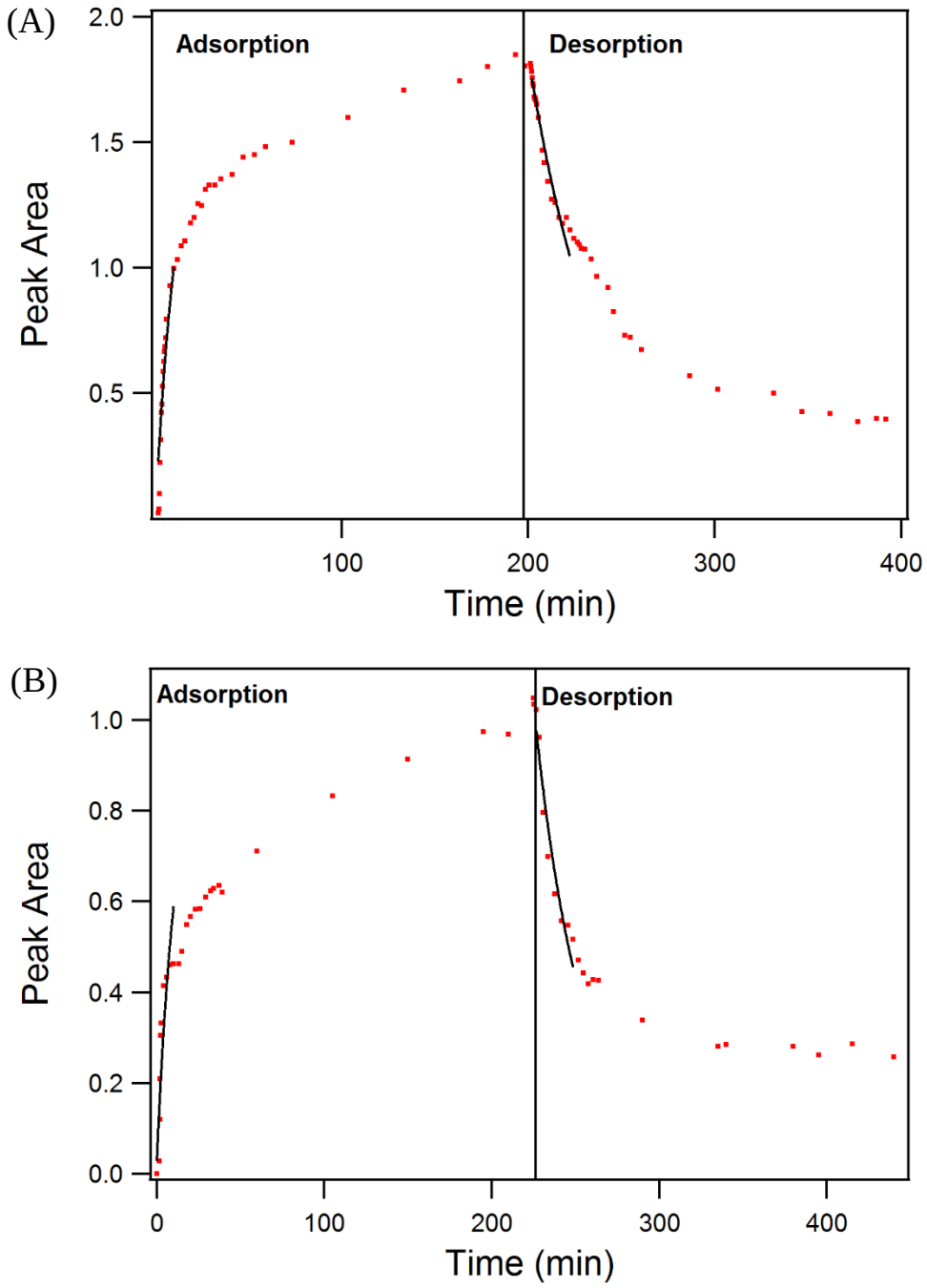


**Figure 4.2:** Adsorption and desorption kinetic curves of 5 mM Lactic Acid on $TiO_2$ nanoparticle surface as a function of pH: (A) pH 5 (B) pH 8. Data points obtained from the peak area between 1506 and 1269 $cm^{-1}$ on ATR-FTIR spectra. Rate constants were determined by fitting exponential decay models to the initial portion of adsorption and desorption kinetic curves, and the fits are shown as the black lines.

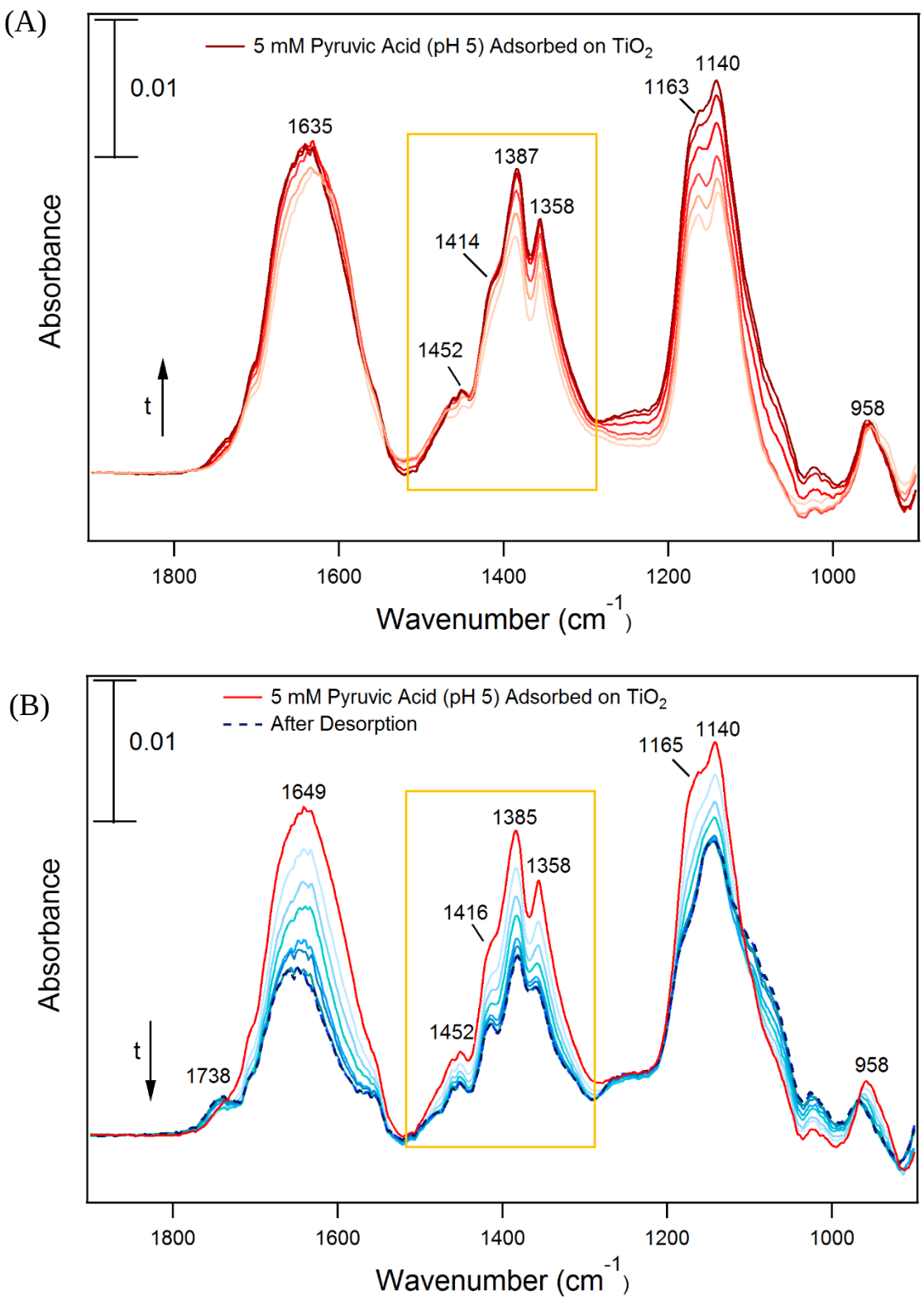


**Figure 4.3:** ATR-FTIR spectra collected every five minutes of 5 mM Pyruvic Acid (pH 5) on $TiO_2$ nanoparticle surface (A) adsorption process (B) desorption process.

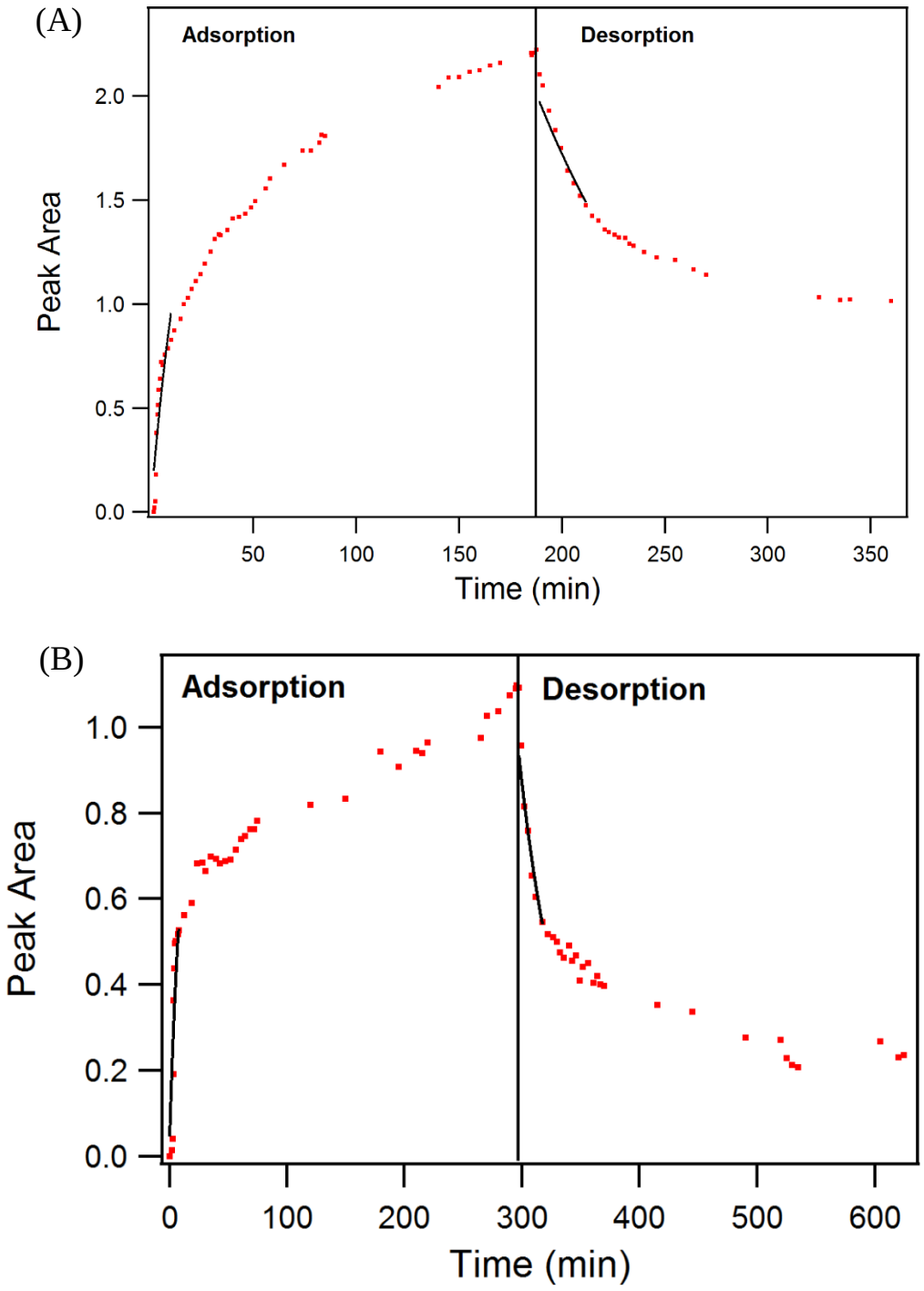


**Figure 4.4:** Adsorption and desorption kinetic curves of 5 mM Pyruvic Acid on $TiO_2$ nanoparticle surface as a function of pH: (A) pH 5 (B) pH 8. Data points obtained from the peak area between 1525 and 1284 $cm^{-1}$ on ATR-FTIR spectra. Rate constants were determined by fitting exponential decay models to the initial portion of adsorption and desorption kinetic curves, and the fits are shown as the black lines.

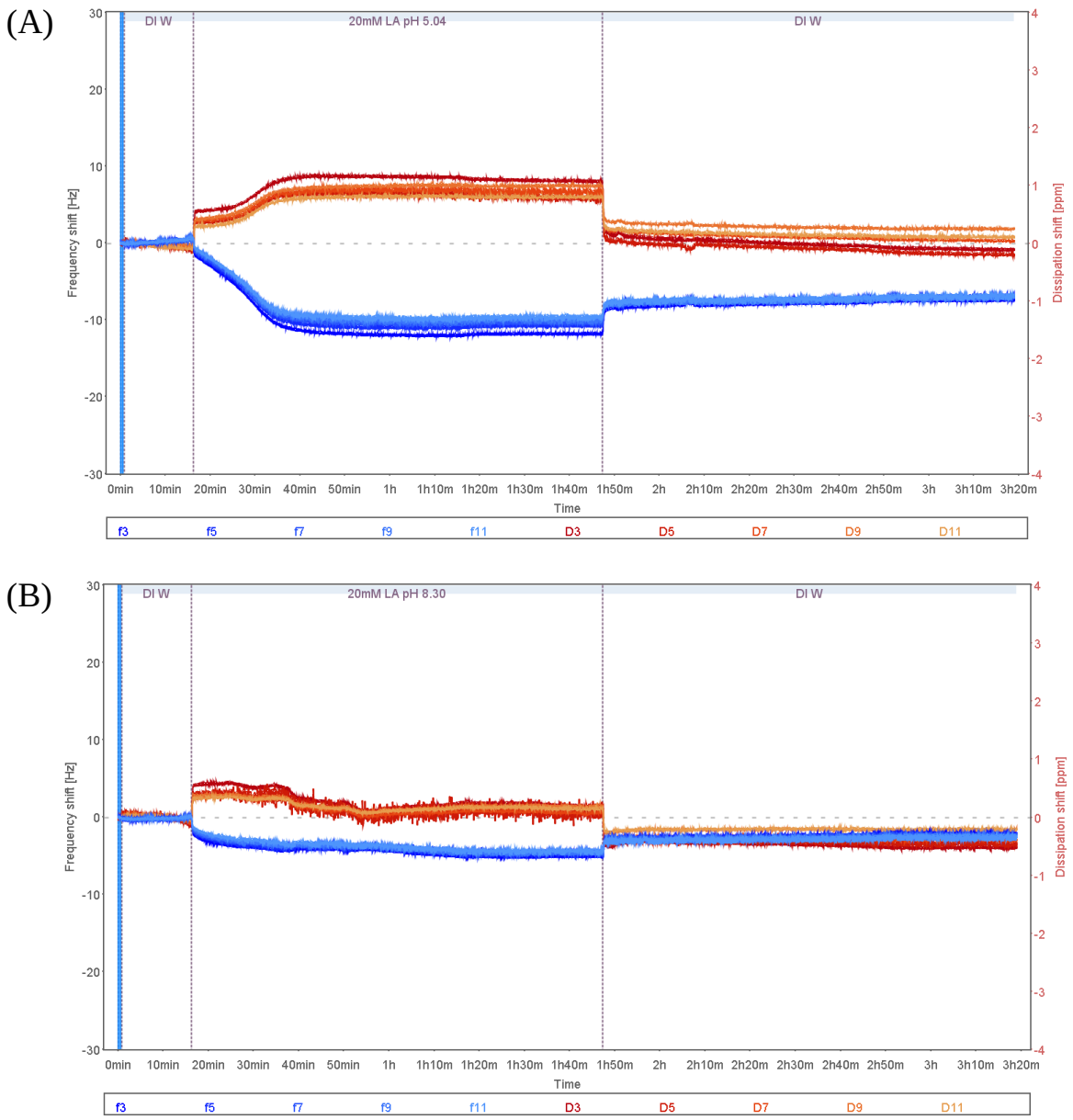


**Figure 4.5:** Shifts in frequency and dissipation, normalized by overtone number, collected over time for the adsorption and desorption of 20 mM Lactic Acid solution adjusted to two indoor-relevant pH values on $TiO_2$ surface: (A) pH 5 (B) pH 8. Data are shown for overtones 3, 5, 7, 9, and 11 in color gradient, in which the darker colors are for the smaller overtones.

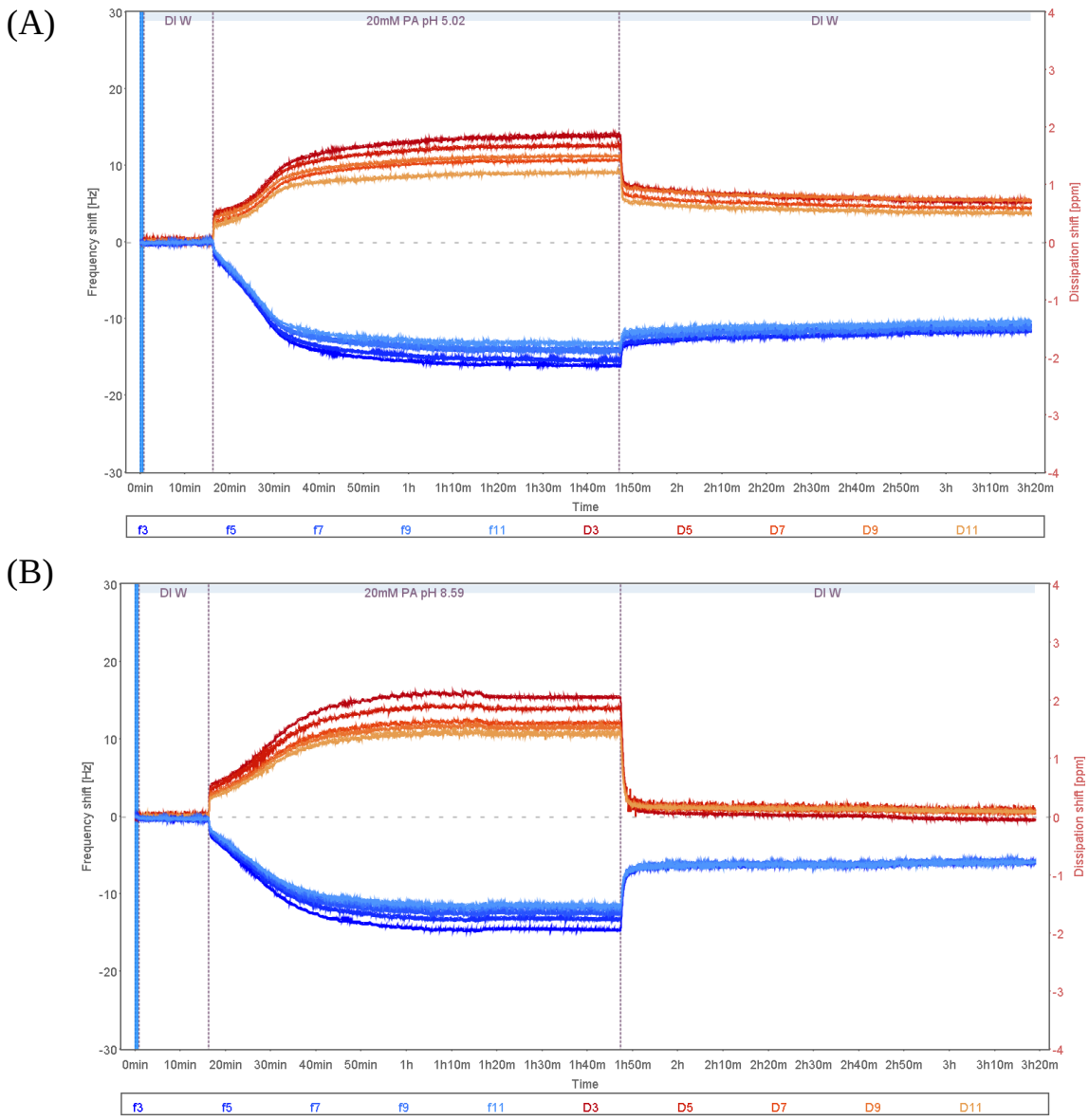


**Figure 4.6:** Shifts in frequency and dissipation, normalized by overtone number, collected over time for the adsorption and desorption of 20 mM Pyruvic Acid solution adjusted to two indoor-relevant pH values on $TiO_2$ surface: (A) pH 5 (B) pH 8. Data are shown for overtones 3, 5, 7, 9, and 11 in color gradient, in which the darker colors are for the smaller overtones.

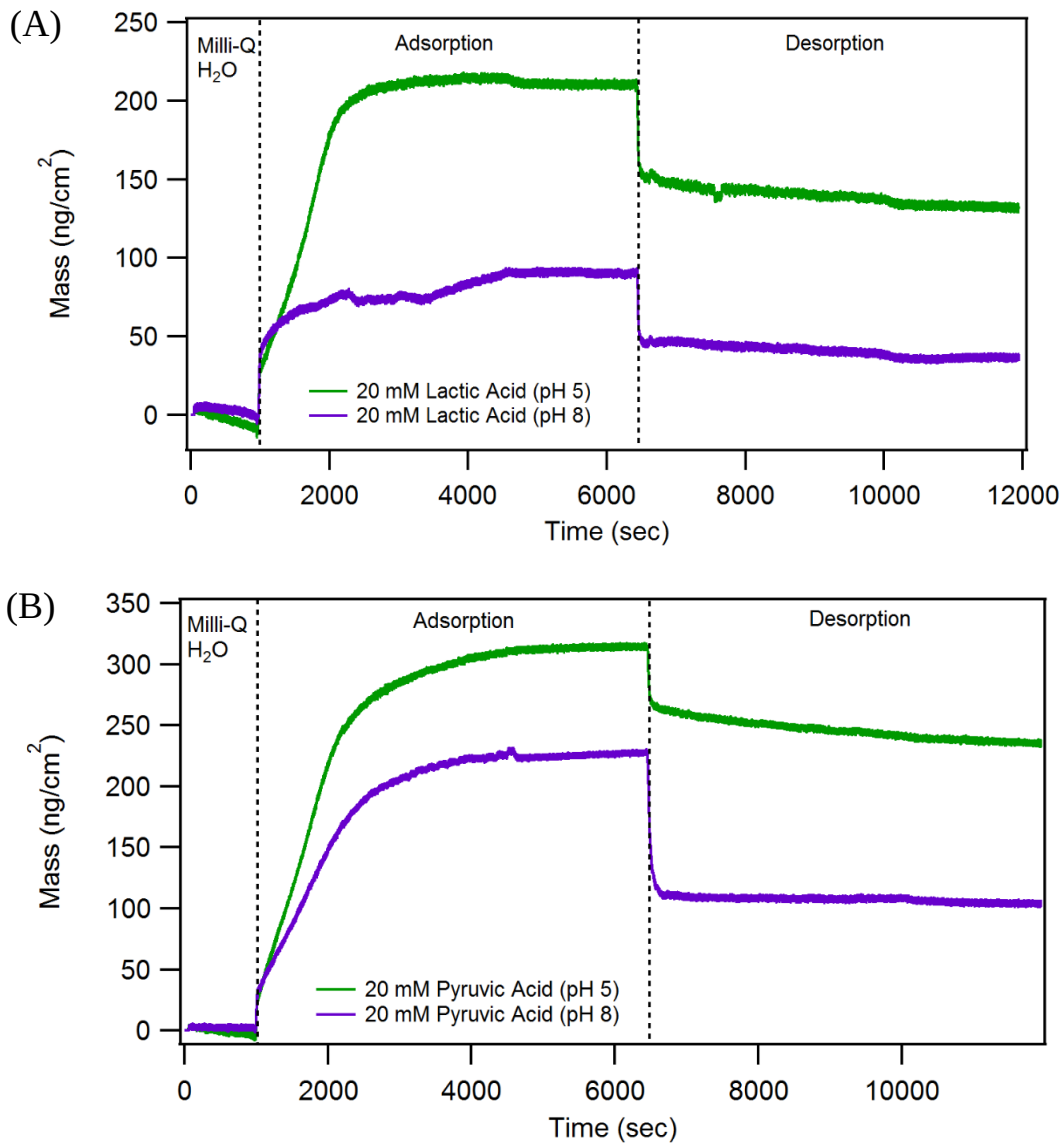


**Figure 4.7:** Mass of adsorbed molecules per $TiO_2$ surface area over time for the adsorption and desorption of (A) 20 mM lactic acid at solution pH 5 (–) and pH 8 (–) (B) 20 mM pyruvic acid at solution pH 5 (–) and pH 8 (–). Measured adsorbed mass per surface area is based on the frequency shift of the third harmonic overtone because it senses the largest surface area across the sensor.

## 4.6 Tables

**Table 4.1:** Adsorption and desorption rate constants determined from experimental kinetic curves of 5 mM Lactic Acid on $TiO_2$ nanoparticle surface at pH 5 and 8.

| 5 mM Lactic Acid Solution pH | Adsorption Rate Constant ($min^{-1}$) | Desorption Rate Constant ($min^{-1}$) |
|---|---|---|
| pH 5 | 0.062 ± 0.005 | 0.0254 ± 0.0009 |
| pH 8 | 0.09 ± 0.01 | 0.035 ± 0.003 |

**Table 4.2:** Adsorption and desorption rate constants determined from experimental kinetic curves of 5 mM Pyruvic Acid on $TiO_2$ nanoparticle surface at pH 5 and 8.

| 5 mM Pyruvic Acid Solution pH | Adsorption Rate Constant ($min^{-1}$) | Desorption Rate Constant ($min^{-1}$) |
|---|---|---|
| pH 5.0 | 0.062 ± 0.005 | 0.012 ± 0.001 |
| pH 8.0 | 0.09 ± 0.01 | 0.027 ± 0.004 |

**Table 4.3:** Calculated number of adsorbed lactate and pyruvate molecules per $TiO_2$ surface area after adsorption and desorption steps at pH values 5 and 8. Range of adsorbed molecules were determined from two QCM-D data sets.

| **Solution pH** | **Lactate Molecules on $TiO_2$ (x $10^{14}$ molecules/$cm^2$)** | | **Pyruvate Molecules on $TiO_2$ (x $10^{14}$ molecules/$cm^2$)** | |
|---|---|---|---|---|
| | **Adsorption** | **Desorption** | **Adsorption** | **Desorption** |
| **pH 5** | 13.0 - 14.3 | 7.91 - 8.99 | 19.9 - 21.9 | 14.4 - 16.5 |
| **pH 8** | 4.76 - 6.22 | 2.22 - 2.50 | 15.8 – 18.1 | 7.26 – 7.40 |

## 4.7 References


1. Roncaroli, F.; Blesa, M. A. Kinetics of adsorption of carboxylic acids onto titanium dioxide. *Phys Chem. Chem. Phys*. **2010**, *12*, 9938-9944.

2. Vogt, B. D.; Lin, E. K.; Wu, W.; White, C. C. Effect of Film Thickness on the Validity of the Sauerbrey Equation for Hydrated Polyelectrolyte Films. *J. Phys. Chem. B.* **2004**, *108*, 12685-126900.

# Chapter 5 Conclusions and Future Studies

## 5.1 Concluding Remarks

The overall goal of this thesis is to study the surface chemistry, adsorption kinetics, and surface coverage of two indoor-relevant carboxylic acids, lactic acid and pyruvic acid, on titanium dioxide surfaces, which is a major component in paints and self-cleaning surfaces, as a function of pH in order to better understand the chemical reactions within indoor environments. These experiments were conducted in the aqueous phase to take into consideration the effect of dampness in residential homes and determine whether the chemistry in aqueous phase reacts differently than in gaseous phase. Chapter 3 discussed the chemistry occurring on the surface upon adsorption of lactic acid at solution pH 3, 5, and 8 and pyruvic acid at solution pH 2.6, 5, and 8. Chapter 4 focused on indoor-relevant pH values and discussed how the kinetic rate constants and surface coverage quantitatively supported the qualitative observations made in the previous chapter. A number of interesting conclusions came from the results of these studies and are summarized in the sections below.

### 5.1.1 Chapter 3 Summary

First, lactic acid and pyruvic acid adsorb onto $TiO_2$ surfaces via deprotonation of the carboxylic group by the surface hydroxyl groups and interactions between the oxygen atoms of $COO^-$ group and two $Ti^{4+}$ atoms on the surface. Lactate and pyruvate are formed and bonded on the surface for all pH values investigated. Second, based on the frequency difference of asymmetric and symmetric stretching vibrations of $COO^-$, lactate and pyruvate bind to $TiO_2$ via bidentate bridging. This type of binding causes a strong electrostatic interaction between the

surface-bound molecules and the $TiO_2$ nanoparticles, which causes the adsorption to be irreversible and thus suggests that chemisorption is occurring on the surface. Third, adsorption intensity of lactic acid and pyruvic acid on $TiO_2$ nanoparticles is pH-dependent. As solution pH increases, intensity of peaks associated with lactate and pyruvate decreases, which suggests that adsorption of lactic acid and pyruvic acid decreases due to increasing repulsion between the negatively-charged $TiO_2$ nanoparticles and anions in the solution phase. Fourth, bulk solution and surface speciation of lactic acid remains constant for pH 3, 5, and 8, but the bulk solution and surface speciation of pyruvic acid differs for pH 5 and 8. Due to the increased fraction of diol species adsorbed on the surface than in solution phase, it is suggested that surface adsorption induces a change in the equilibrium of ketone and diol species.

### 5.1.2 Chapter 4 Summary

First, the reaction order for the adsorption-desorption process of lactic acid and pyruvic acid on $TiO_2$ is pseudo first order, and the rate constants were determined by fitting the exponential decay model to the initial portion of the kinetic curves. Second, adsorption and desorption rate constants do not significantly differ as solution pH increases. Third, QCM-D experiments show that surface coverage of lactic acid and pyruvic acid molecules on $TiO_2$ decreases as solution pH increases, which supports the qualitative observations obtained from ATR-FTIR studies.

## 5.2 Future Work

While the work in this study helped to better understand the chemistry of lactic acid and pyruvic acid on $TiO_2$ surfaces, much more work remains to be done. With the use of mass spectrometry, formation of other species upon adsorption of lactic acid and pyruvic acid on $TiO_2$

can be determined. A previous study has shown that lactic acid in the gas phase on $TiO_2$ may undergo a dehydrogenation reaction and dissociate to form additional surface products like 2-oxy-propionic acid, so the formation of this compound in the aqueous phase can be verified with mass spectrometry.[1] In addition, only the effect of dampness and pH were investigated in this study, so other environmental factors that can affect chemical reactions in indoor environments should be examined. For example, the role of light for these reactions can be investigated. Pyruvic acid adsorption on $TiO_2$ in the gas phase has shown that photochemical products are formed on the surface when illuminated, so it will be interesting to determine whether the same photochemical products are present in the aqueous phase or if different products are formed due to the presence of ketone and diol species in solution.[2] Lastly, there are a multitude of compounds identified in indoor environments, so similar studies with other indoor-relevant compounds can be performed.

## 5.3 References


1. Chen, Y. K.; Lin, Y. F.; Peng, Z. W.; Lin, J. L. Transmission FT-IR Study on the Adsorption and Reactions of Lactic Acid and Poly(lactic acid) on $TiO_2$. *J. Phys. Chem. C.* **2010**, *114*, 17720-17727.

2. Alves, M. and Fang, Y.; Wall, K.; Grassian, V. H. Surface Chemistry and Photochemistry of Pyruvic Acid on Oxide Surfaces. *In preparation.*